

1 CIAO observatory main upgrade: building-up an ACTRIS compliant 2 aerosol in-situ laboratory

3 Teresa Laurita¹, Alessandro Mauceri¹, Francesco Cardellicchio¹, Emilio Lapenna¹, Benedetto De Rosa¹,
4 Serena Trippetta¹, Michail Mytilinaios¹, Davide Amodio¹, Aldo Giunta¹, Ermann Ripepi¹, Canio
5 Colangelo¹, Nikolaos Papagiannopoulos¹, Francesca Morrongiello¹, Claudio Dema¹, Simone Gagliardi¹,
6 Carmela Cornacchia¹, Rosa Maria Petracca Altieri¹, Aldo Amodeo¹, Marco Rosoldi¹, Donato Summa¹,
7 Gelsomina Pappalardo¹, Lucia Mona¹

8
9 ¹Consiglio Nazionale delle Ricerche – Istituto di Metodologie per l’Analisi Ambientale CNR-IMAA, C. da S. Loja, Tito
10 Scalo, Potenza, 85050, Italy

11 *Correspondence to:* Teresa Laurita (teresa.laurita@cnr.it)

12 Abstract

13 This paper describes the aerosol in-situ laboratory at the CNR-IMAA (Consiglio Nazionale delle Ricerche – Istituto di
14 Metodologie per l’Analisi Ambientale) Atmospheric Observatory (CIAO) in South Italy, outlining its configuration and
15 detailing each instrument and sampling lines. The CIAO observatory has been collecting observations of atmospheric
16 components since 2000. Initially the activities revolved around aerosol lidar, later radiosounding and cloud remote sensing
17 observations were added over the years and made CIAO a leading atmospheric observatory in the Mediterranean region. In
18 2018, a significant upgrade started for enhancing the observational capability by adding aerosol in-situ instruments, with the
19 objective to push new research boundaries for aerosol particles characterization and multi-instrumental combined approaches.
20 Here, we describe each technical implementation step for building up an extensive aerosol in-situ laboratory compliant with
21 ACTRIS (Aerosol Clouds and Trace gases Research InfraStructure) standard operating procedures. Starting from scratch, the
22 long path initiated in 2018, with the design of the laboratory in terms of instruments, container layout, inlets and sampling
23 lines, that required time and interactions with experts in the field. Reporting here all the details about the final solutions
24 implemented at CIAO, this paper will be, for new aerosol in-situ laboratory, a practical guide for the implementation of the
25 aerosol in-situ observational site.

26 **1 Introduction**

27 The importance of a quantitative and qualitative assessment of atmospheric aerosol particle characteristics has been recognized
28 since many years: aerosol particles are responsible for direct and indirect effects on atmospheric processes, affecting climate
29 and human health, as well as precipitation cycle and air quality (e.g. Pöschl, 2005; Ren-Jian et al., 2012; IPCC, 2021).
30 Depending on their sources, aerosol particles appear in different sizes/shapes and their relatively short lifetime makes the
31 physical and chemical properties extremely variable both on temporal and spatial scales. Because of the inherent complexity
32 of aerosol particles, a single measurement technique providing all the relevant information is not available: thus, a multi-
33 instrument approach is needed. The combination of different techniques and observational platforms can be crucial for a better
34 understanding of the presence and the characteristics of atmospheric aerosol particles, as well as their role in the large variety
35 of processes in which they are involved. The Aerosol Clouds and Trace Gases Research InfraStructure (ACTRIS,
36 www.actris.eu; Laj et al., 2024) is the European Research Infrastructure (RI) aiming to integrate previous existing networks
37 for the characterization of aerosol particles, clouds and trace gases using and integrating in-situ and remote sensing
38 observations, and experimental platforms for the characterization of atmospheric components under controlled environments.
39 An overarching investigation of the atmosphere which accounts for all these three components is a winning strategy: For
40 instance, aerosol particles act as cloud condensation nuclei (CCN) affecting the cloud properties and lifetime; emitted gas
41 species may act as precursors to form new particles in the atmosphere, i.e., the secondary aerosol particle. Integrated
42 approaches of remote sensing and in-situ observations allows to take the most from the detailed and accurate characterization
43 in terms of morphology of particles, dimension and chemical composition: the remote sensing provide the vertical profile of
44 physical and optical properties information which are essential for investigating aerosol layers, long range transportation,
45 mixing processes and aerosol-cloud interactions; the latter is the only approach to provide the chemical composition and
46 reliable data at ground level, where aerosol particles affect ecosystems and humans.

47 In this scenario, the CNR-IMAA Atmospheric Observatory (CIAO; Madonna et al., 2011), operating since 2000, has been
48 recently upgraded with the aerosol in-situ observational component, thus complementing the multi-year high-quality aerosol
49 remote sensing data record. The combination of the aerosol in-situ measurements with remote sensing observations is expected
50 to strengthen fundamental knowledge about aerosol particle impact on human health, ecosystems, and climate. This
51 combination can be achieved either by comparing or complementing the techniques: the results of the comparison will allow
52 to reduce the uncertainty of aerosol particles measurements in the atmosphere, with a subsequent improvement of model
53 predictions on climate change, whereas the complementarity results in the possibility of investigating the aerosol particles
54 from the ground up to the stratosphere. The new aerosol in-situ facility at CIAO, funded by the Italian Ministry of University
55 and Research through the PER-ACTRIS-IT project (<https://www.imaa.cnr.it/en/projects/38-attivita/progetti/713-per-actris-it>,
56 last access: 6 December 2023), has received initial acceptance as ACTRIS National Facility observational platform for the

57 measurements of at least the obligatory ACTRIS aerosol in-situ variables. The site has begun the next phase of the labelling
58 process in 2024, a key element of ACTRIS's data quality assurance system. This process ensures that instruments, data, and
59 methodologies used across ACTRIS observational platforms meet specific quality criteria. The labelling process involves a
60 series of evaluations and certifications to verify compliance with ACTRIS protocols (Deliverable 5.1: ACTRIS NF Labelling
61 Plan). During the labelling process, the National Facilities are annually invited by CAIS - ECAC (Center for Aerosol In-Situ –
62 European Centre for Aerosol Calibration and Characterization) to calibration workshops, where instruments are calibrated,
63 and the quality of the data is thoroughly verified.

64 In this paper we present a concise overview of the observatory, focusing on the characteristics of the recently established
65 ACTRIS-compliant in-situ facility, with the main aim to benefit the aerosol community providing a comprehensive and
66 detailed description of technical solutions for the implementation of such component. A guidance for building-up an ACTRIS
67 aerosol in-situ station, it is potentially of interest also for extra European/outside of ACTRIS community: the ACTRIS in situ
68 standards are in some way following the WMO/GAW (World Meteorological Organization/Global Atmosphere Watch;
69 WMO/GAW, 2016) ones, therefore the interest in technical solutions for an ACTRIS compliant in-situ instrumentations stays
70 not only with the stations potentially involved in ACTRIS. Additionally, new EU air quality directive will include some more
71 advanced stations where black carbon and ultrafine measurements should be collected. Therefore, solutions adopted for
72 collecting such measurements with ACTRIS standard could be of interest for air quality management networks for guarantying
73 the quality of the collected data.

74 After a short description of CIAO and typical atmospheric conditions in Sect. 2, Sect. 3 reports about the remote sensing
75 instrumentation currently operating at CIAO. Section 4 represents the core of this paper, providing the in-depth description of
76 the in-situ facility with the detailed configuration of each instrument and sampling lines. Finally, Sect. 5 illustrates three
77 scientific topics to be studied at CIAO with the combined deployment of aerosol in-situ and remote sensing measurements.²

78 Description of the site

79 Equipped with state-of-the-art systems for remote-sensing and in-situ measurements of aerosol particles, CIAO
80 (<https://ciao.imaa.cnr.it>, last access: 4 December 2023) is currently a reference station for short-live atmospheric constituents
81 in Italy and the Mediterranean. The site is located on the Southern Apennine in Italy (Tito Scalo, 40.60° N, 15.72° E, 760 m
82 a.s.l.), in a plain surrounded by low mountains, less than 150 km away from the West, South and East coasts (Fig. 1).

83
84
85

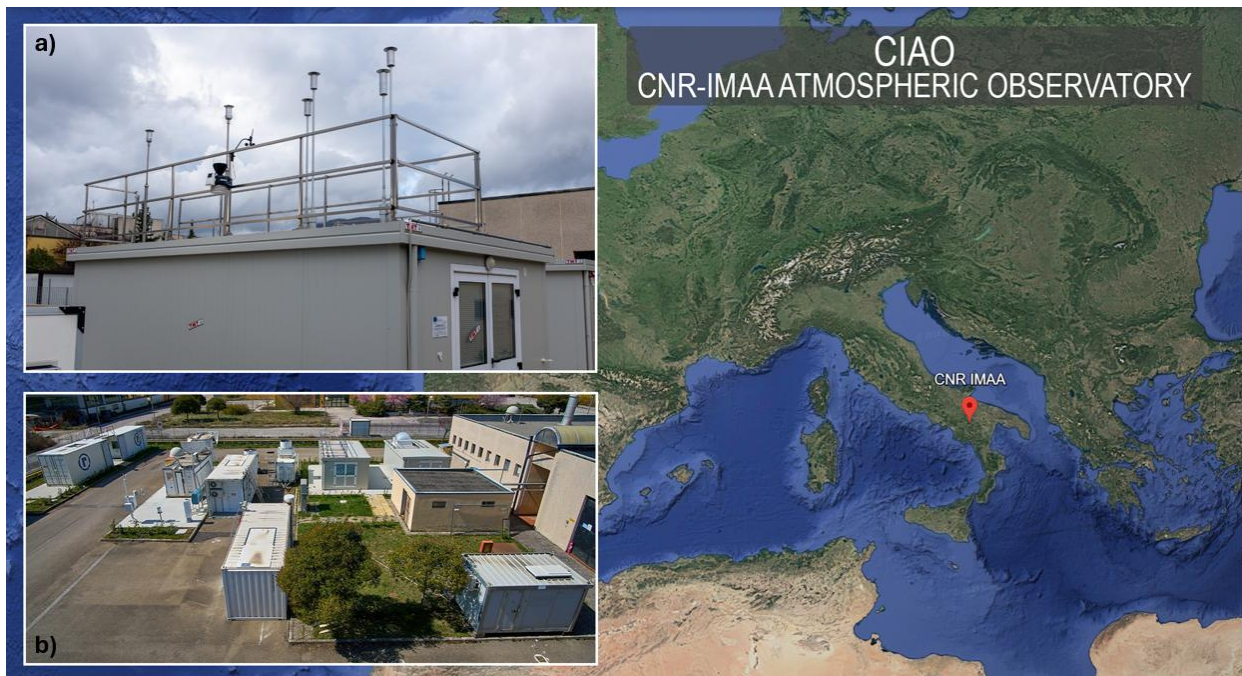


Figure 1: Location of the CNR-IMAA Atmospheric Observatory (© Google Earth); a) overview of the aerosol in-situ facility and b) overview of all CIAO infrastructures.

Therefore, it operates in a typical mountainous weather strongly influenced by Mediterranean atmospheric circulation, resulting in generally dry, hot summers and cold winters. Indeed, dew point temperatures at the station between 2004 and 2017 after sunset exceeded 15°C only during summer (Fig. 2). The prevailing wind direction occurring at the site is W-WSW-SW (Fig. 3).

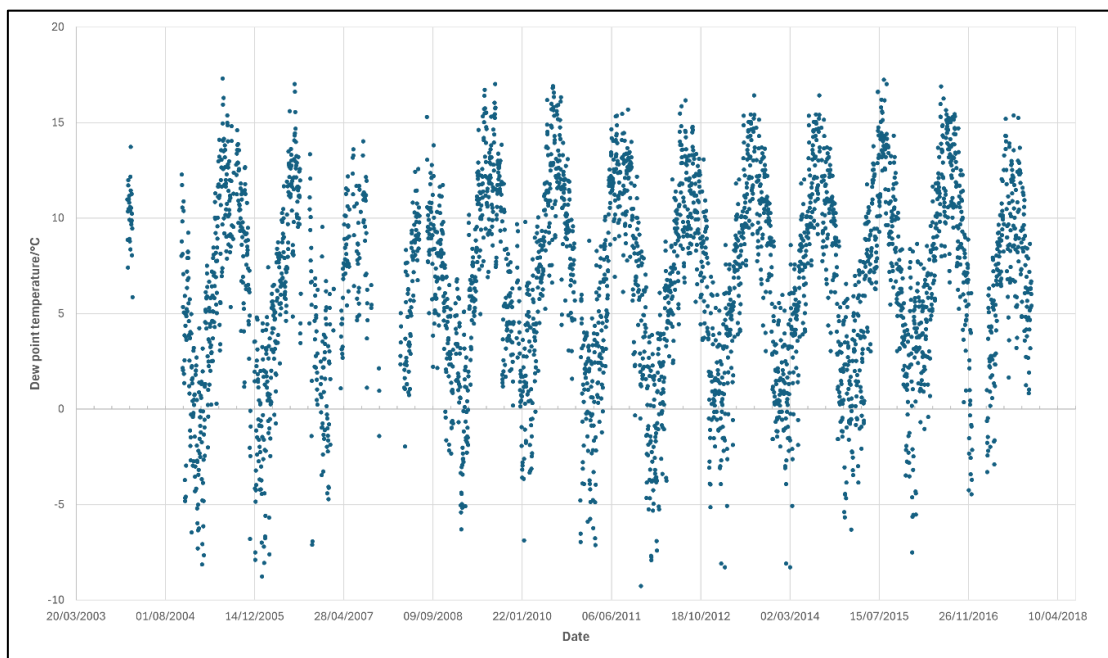


Figure 2: Dew point temperature time series at CIAO in the timeframe 2004-2017 obtained from continuous measurements of the automatic weather station VAISALA MILOS520 with daily mean.

Most of the surrounding land is classified as arable crops in non-irrigated areas, followed by broad-leaved woods and coniferous forests, sclerophyllous or wooded/shrubby areas and natural grazing areas and grasslands (<http://rsdi.regione.basilicata.it>, last access: 28 November 2023).

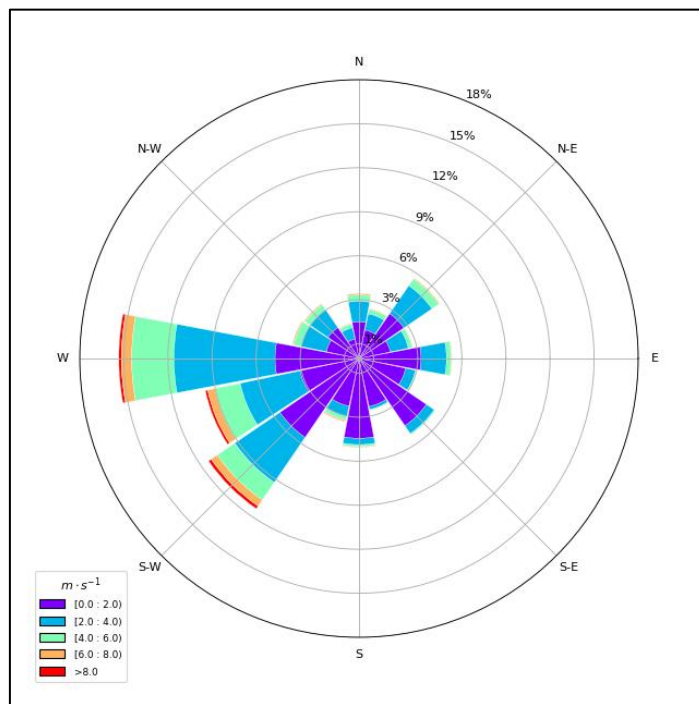


Figure 3: Wind rose diagram at CIAO in 2004-2017 obtained from continuous measurements of the automatic weather station VAISALA MILOS520 with temporal resolution of 1 minute.

CIAO's mission is to improve the knowledge of atmospheric processes and their role in meteorological phenomena, climate change and air quality. Given the coverage and global relevance of the processes studied, fundamental aspects of the activities and approaches adopted are the development of internationally recognized Standard Operating Procedures, the open data policy and the full sharing of methodologies and know-how.

CIAO provides free and open access to national and international users like researchers, small and medium-sized enterprises (SMEs), students and citizens. At the present time, CIAO extends its outreach through the ATMO-ACCESS Trans-National Access program (<https://www.atmo-access.eu/second-call-for-access/>, last access: 2 December 2023). This program allows participants to engage in research on aerosol particles and their effects, to learn techniques and methods, to contribute instruments, or to collaborate with the team.

The research activities of CIAO evolved within the long-term observations of aerosol particles, clouds, trace gases and greenhouse gases within the European research infrastructures ACTRIS and ICOS (Integrated Carbon Observing System), as well as around the participation of CIAO in reference observational programs and networks on a global scale, such as GRUAN (GCOS (Global Climate Observing System) Reference Upper-Air Network) and GALION (GAW Aerosol Lidar Observation

Network). The observational strategy is organized to provide quality assured data for satellite validation and model evaluation and to fully exploit the synergy and integration of the active and passive sensors for the improvement of the atmospheric characterization (e.g., Pappalardo et al., 2004; Mona et al., 2009; Boselli et al., 2012; Ilić et al., 2022). The complete list of CIAO publications is available at <https://ciao.imaa.cnr.it/publications/>.

For what concerns aerosol particles measurements, CIAO due to its geographical position as well as the low aerosol particles background concentration is interesting for studying particles of natural origin such as desert dust and volcanic ash clouds. The site is regularly affected by Saharan dust intrusions (e.g., Mona et al., 2006; Mona et al., 2014; Biniotoglou et al., 2015; Soupiona et al., 2020) has been reached by volcanic aerosol particles at the level of free troposphere during the eruptions of Etna (e.g., Pappalardo et al., 2004a, Villani et al., 2006) and Eyjafjallajökull (Madonna et al., 2010; Mona et al., 2012; Pappalardo et al., 2013) volcanos in 2002 and 2010, respectively, and stratospheric layers (e.g., Sawamura et al., 2012). In recent years, the observatory has become actively involved in the study of smoke plumes originated by wildfires occurring both at short-range, spreading with increased frequency in the surrounding forestry areas during the summer period (De Rosa et al., 2022), and long-range transported plumes, such as the autumn 2020 California wildfires whose smokes transported in the stratosphere reached the site within 13 days (Baars et al., 2019).

3 Remote sensing measurements

Remote sensing measurements have been the backbone of the research activity at CIAO since its beginning in the early 2000s, with the scientific goal of providing long-term measurements for the climatology of aerosol and cloud properties.

Besides the compliance to the ACTRIS guidelines, all the remote-sensing measurements performed at CIAO are designed to be in line with the main ground-based observation networks (i.e., EARLINET (European Aerosol Research Lidar Network to Establish an Aerosol Climatology), CloudNet, AERONET (AERosol RObotic NETwork), GRUAN, GALION) and the major international standards provided by the WMO/GAW 2016, aiming at establishing a long-term, harmonised and statistically significant database of measurements of atmospheric parameters and constituents for climatological studies (Matthias et al., 2004).

The active remote-sensing instruments operative at CIAO include multi-wavelength Raman and polarization lidars, ceilometers, Doppler lidars and polarimetric Doppler radars, and the passive ones include microwave radiometers, photometers, and a high-resolution Fourier-Transform Infrared (FTIR) spectrometer.

With respect to the status of CIAO reported in previous papers (e.g., Madonna et al., 2011), some instruments are still operating, some have been replaced by more recent and advanced ones, and new instruments for increasing the observational capabilities have been added.

152
153
154
155
156
157
158
159
160
161
162
163
164
165
166
167
168
169
170
171
172
173
174
175
176
177
178
179
180
181

For the aerosol remote sensing, two new highly-advanced lidar systems have been recently installed at CIAO, one fixed and one mobile.. They are able to provide measurements of vertical profiles of several aerosol optical properties: backscatter coefficient and particle depolarization at 1064, 532 and 355 nm, and extinction coefficient at 532 and 355 nm, with the observational range starting from 200 m up to at least 20 km of altitude. The two systems are reference lidars for ACTRIS and offer services to test the performances of other lidar systems also through on-site direct intercomparison campaigns using the mobile lidar.

Close by to the aerosol multiwavelength depolarization Raman, a triple mode photometer is operational within AERONET and ACTRIS providing columnar aerosol optical depth measurements and columnar size distribution information not only in daytime, but also in night-time under certain illumination conditions. CIAO is also equipped with a lidar laboratory and an optical laboratory, which allow to implement and test several and customized lidar configurations and to test and characterize optical components and laser sources typically used in high power lidar systems.

Besides the aerosol remote sensing instruments, cloud remote sensing equipment has also been updated and expanded with additional complementary instruments, and a high resolution FTIR spectrometer has been added for performing remote sensing measurements of trace gases to complement the other observations.

The availability of a large number of remote-sensing systems at the observatory has enabled the possibility to both compare and combine different techniques for studying atmospheric parameters (e.g., Mona et al., 2007; Madonna et al., 2010; Boselli et al., 2012; Lopatin et al. 2013; Madonna et al., 2015).

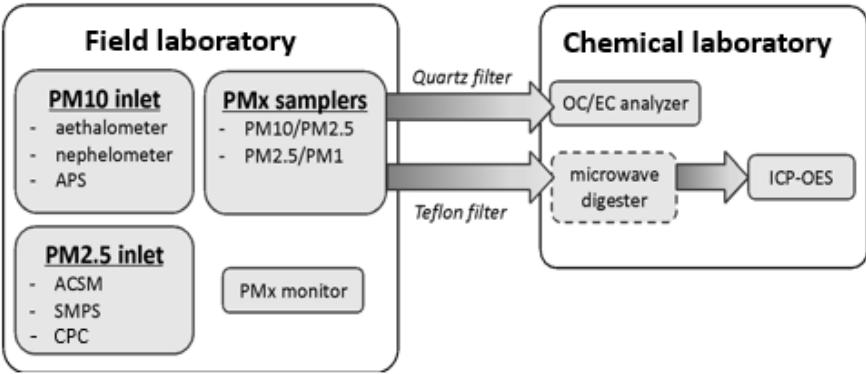
Synergistic approach has been proposed for the study of thin liquid water clouds, combining multi-wavelength lidar and Doppler radar measurements (Rosoldi et al., 2022). It has been shown that microwave radiometer can be used to calibrate Raman lidar measurements for water vapour profiling and that the synergy between these instruments is an effective means for atmospheric water vapour monitoring (Madonna et al., 2006, Mona et al., 2007).

However, despite its huge potential in atmospheric research, there are two major drawbacks associated with the remote sensing observations: the inability to conduct aerosol measurements under skies with low clouds and precipitations, along with the impossibility of characterising the particulate properties near the ground. Therefore, the recent implementation of the in-situ facility described in the next section is fundamental to achieve a complete characterization of the aerosol at the ground level where the aerosol particles directly affect ecosystems and human health. In addition, the in-situ measurements include the valuable chemical characterization of the particulate matter (PM), thus providing a deeper comprehension of the aerosol type, the source apportionment and the mixing atmospheric processes.

182 **4 Description of the aerosol in-situ facility**

183 **4.1 Overview**

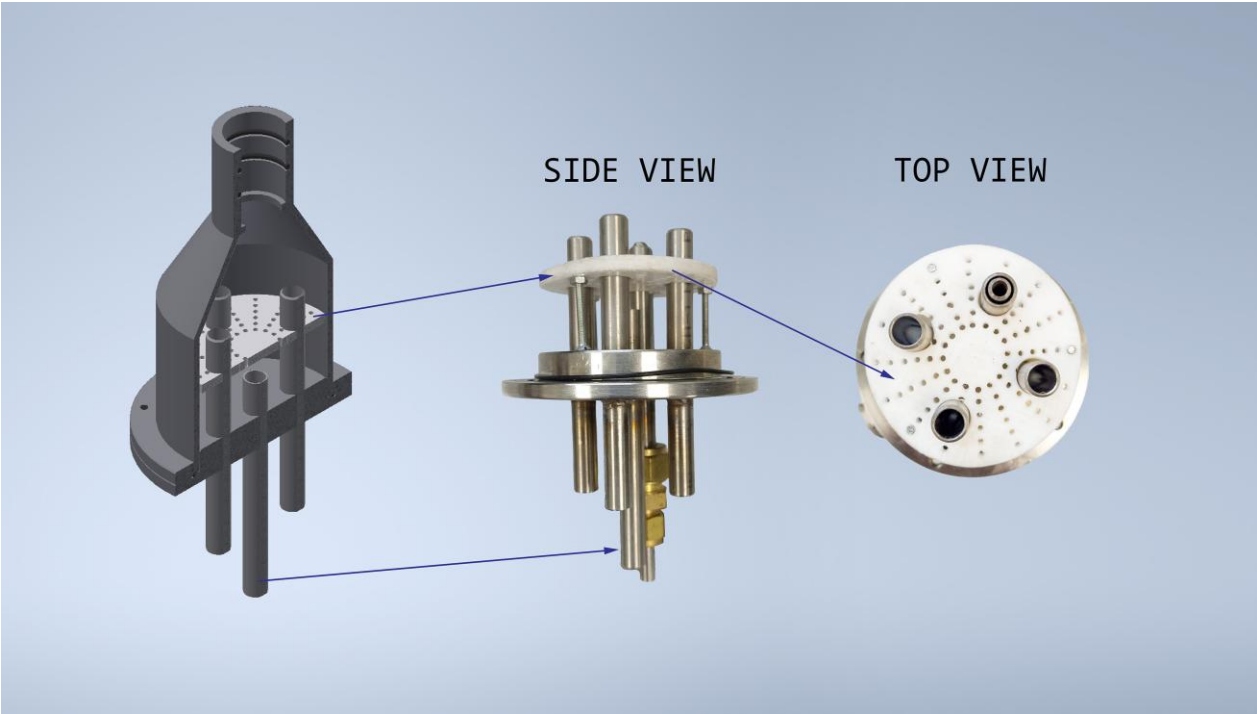
184 The in-situ facility recently installed at CIAO comprises two main parts (Fig. 4): a field laboratory for aerosol particles online
185 measurements with continuous instrumentation and PM samplers and a chemical laboratory for the post-sampling analysis of
186 aerosol particles collected on filters. This facility enables the measurement of all obligatory ACTRIS aerosol in-situ variables:
187 particle number concentration > 10 nm; particle number size distribution – mobility diameter 10 to 800 nm; particle light
188 scattering & backscattering coefficient and particle light absorption coefficient and equivalent black carbon concentration.
189 Additionally, it allows the measurement of other four recommended variables: particle number size distribution - aerodynamic
190 diameter 0.8 to 10 µm; mass concentration of particulate organic and elemental carbon; mass concentration of non-refractory
191 particulate organics and inorganics and mass concentration of particulate elements.



194
195 **Figure 4: Outline and workflow of the aerosol in-situ facility at CIAO.**

196
197 The shelter has been designed according to the ACTRIS guidelines and recommendations (Wiedensohler et al., 2014), with
198 the instrumentation arranged as follows: a dual spot aethalometer (AE33, Magee Scientific), a multi-wavelength integrating
199 nephelometer (AURORA 3000, Ecotech) and an aerodynamic particle sizer (APS 3321, TSI) located downstream a common
200 PM₁₀ (aerosol particles with an aerodynamic diameter less than 10 µm) inlet; a time-of-flight aerosol chemical speciation
201 monitor (ToF-ACSM, Aerodyne Research), a scanning mobility particle sizer (SMPS3938, TSI) and a condensation particle
202 counter (CPC3750, TSI) placed downstream a PM_{2.5} (aerosol particles with an aerodynamic diameter less 2.5 µm) common

inlet. Additionally, two PM_x samplers (SWAM 5a-Dual Channel Monitors, FAI Instruments) are installed with respective inlets: one equipped with two PM_{2.5} inlets, and the other with one PM₁₀ and one PM₁ inlet. Furthermore, a PM_x monitor (EDM 180, Grimm) is placed as a standalone instrument with individual PM₁₀ inlet line. Particular attention has been devoted to the design of the common inlets and the sampling lines. The PM₁₀ and PM_{2.5} common impactor type inlets, operating at a flow rate of 16.7 l min⁻¹, are compliant with EN 12341 and EN 14907 standards, respectively. The main challenge when transporting aerosol particles to collectors and aerosol particles measuring instrumentation is to avoid particles losses. Therefore, firstly, the internal diameter of the main sampling pipe of the common PM₁₀ and PM_{2.5} inlets must be such as to ensure that the sampled air has a laminar flow along the entire path (Reynolds number less than 2000) to minimise the loss of particles by diffusion and inertia. The instrument sublines (characterised by smaller inside diameters) are connected to the two common PM₁₀ and PM_{2.5} inlets through their respective isokinetic flow splitter (Fig. 5), where the sample flow velocity closely matches the velocity of the main flow. Moreover, the tube ends in the isokinetic flow splitters must be sharp to minimize turbulence and promote smooth airflow, ensuring uniform sampling. This design helps maintain laminar flow, reduces aerosol losses, and enhances the accuracy and reliability of measurements. Another key feature of the splitter is that the sample is collected from the core of the main aerosol flow rather than from streamlines near the wall of the main pipe, therefore, ensuring a representative sampling (especially for coarse and nanoparticles).



219
220 **Figure 5: Image showing the rendering 3D of the isokinetic splitters, including the side view and top view** (<http://www.quattro->
221 [esse.it/Home.html](http://www.quattro-esse.it/Home.html)).
222

223 The technical details of the common inlets and isokinetic splitters are shown in Table 1.
224

Common Inlet					Isokinetic splitter				
Inlet	Flow rate (l min ⁻¹)	Int. Diameter (mm)	Speed (m s ⁻¹)	Reynolds Number	Instrument	Int. Diameter (mm)	Flow rate (l min ⁻¹)	Reynolds Number	Speed (m s ⁻¹)
PM 10	16.7	21.2	0.8	1135	Aethalometer	8	5	885	1.6
					Nephelometer	8	5	885	1.6
					APS	4.4	1	320	1.09

PM 2.5	16.7	21.2	0.8	1135	SMPS	4.4	2	655	2.2
					CPC				
					ToF-ACSM	8	3	530	1

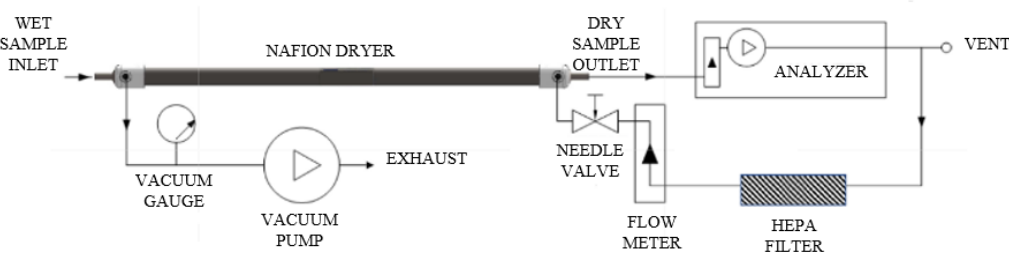
Table 1: Technical details of the common inlets and isokinetic splitters.

All the sampling tubes are kept as short as possible and are placed in vertical position with bends and connectors avoided as much as possible to suppress potential sources of turbulence, which would result in additional losses of particles. In addition, in accordance with ACTRIS recommendations, the tubes used are black sampling tubes supplied by TSI company (<https://tsi.com/home/>). These TSI sampling tubes are made of conductive silicone, infused with carbon black to improve conductivity. This design is essential to minimize electrostatic losses, which can occur in non-conductive tubes, such as those made of standard silicone or Teflon, where particles can adhere to the tube walls due to static charges. The conductive nature of TSI tubes prevents the buildup of electrostatic fields, thus improving particle penetration and reducing sampling distortions caused by particle loss. The inlets on the rooftop of the field laboratory are placed at one metre from each other and height of 1.5-2.0 m above the roof, corresponding to approximately 4.5–5 m above ground level, with the aim of minimising local influences and potential interferences in the sampling process.

In compliance with the ACTRIS indications, all the instruments in the laboratory are equipped with a Nafion dryer tube, a specialized device made from a sulfonated tetrafluoroethylene-based polymer. This device is used in aerosol sampling to remove water vapor from the gas stream while preserving the chemical integrity of aerosol particles (Monotube Dryer 700 (MD-700) - Perma Pure). These Nafion dryers maintain the RH well below 40%; under this threshold, in fact, changes in particle diameter due to RH variations are expected to be lower than 5%, thus obtaining comparable data, independent of the hygroscopic behaviour of the aerosol particles. Moreover, the upstream drying prevents the possible instrument damage caused by water condensation.

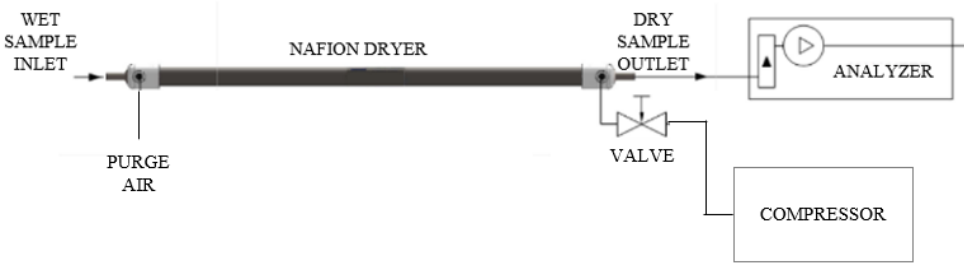
The Nafion dryers of Aethalometer, Nephelometer, APS and ACSM operate in a reflux mode, shown in Fig. 6, which returns the dry sample back to the dryer for use as the purge after it has gone through the analyzer. Since this method uses all the dry sample as purge air, only the sample flow required for analysis passes through the dryer. This results in a high drying efficiency. The vacuum on the purge air should be at least 15 inches Hg, with a higher vacuum preferable. This vacuum level is required to provide the desired 2:1 purge-to-sample flow ratio based on the actual volumetric flow. The 2:1 ratio ensures enough dry purge gas to continuously absorb moisture, preventing saturation and preserving sample integrity. This is crucial in aerosol

249 particulate sampling, where even small amounts of moisture can affect particle characteristics and compromise measurement
250 accuracy.
251



252
253 **Figure 6: Schematic Diagram - Nafion Reflux mode** (MD-700-User-Manual, <https://www.permapure.com>).

254 In contrast, the Nafion dryer connected to the SMPS and CPC cannot operate in reflux mode but operates in counter flows
255 using air dry coming from a compressor (Acoem 8301 LC-H Zero Air Generator), since the instruments need n-butanol as a
256 working liquid for the growth of aerosol particles. (Fig. 7).



257
258 **Figure 7: Schematic Diagram - Nafion counter flows mode.**
259

260 Moreover, at the inflow of each instrument, there is a high-resolution sensor connected to a software for continuous monitoring
261 (every minute) of relative humidity and temperature. The accuracy of the sensors is 2.5% for the RH and 0.5°C for the
262 temperature.

263 Lastly, in order to limit the temperature variation around the instruments, a continuously operating air conditioning system set
264 at 23°C has been installed in the laboratory.

265 As previously mentioned, the in-situ facility is complemented by the chemical laboratory which enables complementary
266 measurements on the particulate matter-loaded filters coming from the PMx samplers, that is not possible to obtain with the

continuous instrumentation. The chemical laboratory include: an inductively coupled plasma optical emission spectrophotometer (ICP-OES, series 5800, Agilent) used to perform the analysis of trace metals, and a multi-wavelength OC/EC analyzer (DRI model 2015, Magee Scientific) used to analyse the carbonaceous fraction of the collected particulate. The implementation of a such wide aerosol in situ measurements facility from scratch has required a total initial investment of about 1M€ and about 2 years, and about 100k€, 2 researchers with the support of a technicians are estimated to be needed to operate the laboratory.

4.2 Instrumentation under the common PM₁₀ inlet

As reported above, a PM₁₀ common inlet is used to feed the aethalometer, the nephelometer and the APS. The aethalometer is a key instrument for wildfire and pollution characterization, being able of detecting the fraction of particulate which absorbs light, known as Black Carbon (BC), formed during the incomplete combustion of carbonaceous matter from biomass burning and fossil fuel (Petzold et al., 2013). According to the ACTRIS guidelines, the AE33 aethalometer operating at seven different wavelengths in the range 370-950 nm is used for the real-time monitoring of the concentration of BC. Briefly, the principle of the aethalometer is to measure at given time intervals the attenuation of a light beam (at 880 nm) transmitted through a filter where the particulate is continuously collected; the rate of change of optical transmission combined with the air flow rate monitored through a mass flowmeter permits to determine the absorption coefficient, then converted into BC concentration by means of the mass-absorption cross section. The dual spot technology refers to the contextual measurement of transmitted light intensities through two separate spots of the filter at different loading levels, thus allowing to compensate for the so-called loading effect largely described by Drinovec et al. (2015). The aethalometer is equipped with a sample stream dryer (Magee Scientific) exploiting a semi-permeable Nafion membrane which keeps the RH well below 40%.

Among the other in-situ instruments placed under the PM₁₀ inlet, the nephelometer can be considered in a certain way complementary to a ground-based lidar, expecting therefore to provide optical parameters consistent with those obtained from the lidar within the atmospheric planetary boundary layer (PBL). However, when the the PBL is particularly shallow (e.g., during wintertime), the nephelometer becomes the only tool to obtain the optical parameters of the aerosol particles residing within the first hundreds of metres from the ground. The ACTRIS-compliant integrating nephelometer AURORA 3000 is used to measure the total scattering (σ_{sp}) and the backscattering (σ_{bsp}) coefficients (integrating within the angular range 9°-170° and 90°-170°, respectively), both correlated to the particle concentration (i.e., extensive properties). The peculiarity of the instrument is the utilisation of a light source emitting at three distinct wavelengths: the light at 635 nm (red) interacts strongly with large particulate matter such as desert dust and sea salt; the light at 525 nm (green) interacts strongly throughout the visible part of electromagnetic spectrum (smog, fog, haze); the light at 450 nm (blue) interacts strongly with fine and ultrafine particulates, such as wood fires and automobile combustion particulate. The nephelometer is equipped with a 36-inch-long

297 Perma Pure Nafion MD-700 in order to prevent condensation of water droplets over the particles, which would increase their
298 size and significantly change their scattering characteristics.

299 Lastly, the APS spectrometer provides high-resolution real-time aerodynamic measurements for the coarse fraction of the
300 particulate (Peters et al., 2003). The optical size range of the APS is from 0.37 to 20 μm , but since the spectrometer is connected
301 to a PM_{10} inlet and the counting efficiency of APS below 0.8 μm aerodynamic diameter rapidly decreases and is unstable, the
302 realistically size range is from 0.8 to 10 μm . The APS is based on the time-of-flight particle sizing, in which the aerodynamic
303 size of a particle determines its rate of acceleration, with larger particles accelerating more slowly due to increased inertia; the
304 time of flight between two laser beams is recorded and converted to aerodynamic diameter using a calibration curve. The
305 instrument measures in parallel the light scattering intensity of the sized particles in the equivalent optical size range from 0.8
306 to 10 μm , thus providing further insights into the aerosol particles nature and composition.

307 The APS is connected to the sampling line just with the inner nozzle (sampling 1 l min^{-1}) from the common sampling line and
308 the flow is dried by a 12-inch Perma Pure Nafion, while taking the additional sheath flow (4 l min^{-1}) from the air compressor.

309 **4.3 Instrumentation under the common $\text{PM}_{2.5}$ inlet**

310 Even though the general ACTRIS recommendations for the in-situ measurements involve the analysis of the PM_{10} fraction,
311 the CPC, the SMPS and the ACSM represent an exception and are more conveniently placed under the cut-off size of a $\text{PM}_{2.5}$
312 inlet. The ACTRIS-compliant CPC is used to measure the number concentration of aerosol particles with diameter > 10 nm.
313 In the CPC, an aerosol sample is continuously drawn through a heated saturator where the butanol is vaporized and diffused
314 into the sample stream. Together, the aerosol sample and *n*-butanol vapour pass into a cooled condenser where the *n*-butanol
315 vapour becomes supersaturated and condenses on the particle surface causing them to grow. The particles are then counted
316 individually as they pass through a laser-based optical detector.

317 Regarding the SMPS, it is an instrument of interest for CIAO, being able to provide the size distribution and concentration of
318 the fine fraction of the particulate in the size range 10 nm – 800 nm. It consists of four components in sequence: 1) a pre-
319 impactor which removes particles larger than the fixed upper limit of size; 2) a bipolar diffusion charger (model 3082, TSI)
320 which confers a characteristic stationary charge distribution to the polydisperse particles by using a radioactive source (Kr-
321 85); 3) a differential mobility analyzer column (DMA, model 3083, TSI) which separates the particles according to their
322 electrical mobility by varying continuously the applied voltage within the column (Schmid et al., 2007); and 4) a condensation
323 particle counter (CPC, model 3750, TSI) where the classified monodisperse particles are counted after condensation of *n*-
324 butanol on their surface.

325 The CPC and the SMPS are connected to the same 24-inch Perma Pure Nafion via a T-flow splitter in order to keep the RH
326 below 40%. Moreover, a dry sheath air is needed for the SMPS to ensure particle sizing inside the DMA with a minimum

327 fluctuation in RH and for this purpose a Silica Dryer Tube (model 3082, TSI) is incorporated in the DMA sheath flow system,
328 which is a closed loop.

329 For what concerns the aerosol particles mass spectrometry techniques, the ToF-ACSM has been shown to be perfectly suited
330 for the ACTRIS observatory platforms. It is specifically designed to provide continuous aerosol particle monitoring over long
331 time periods, spanning years, with the requirement of regular checks and calibrations to maintain the accuracy and reliability
332 of its long-term measurements. The chemical speciation with high temporal resolution is a unique feature of the ACSM
333 technology, unobtainable with conventional filter sampling and subsequent post-processing chemical methods; moreover, the
334 ACSM is not subjected to sampling artefacts that affect the collection of semi-volatile PM components by means of filters
335 (Viana et al., 2006; Kim et al., 2015). The ToF-ACSM chosen for CIAO was introduced in 2013 (Fröhlich et al., 2013),
336 providing a higher mass resolution (i.e., $m/\Delta m = 600$) and superior detection limits (i.e., less than nanograms per cubic meter)
337 with respect to the previously developed quadrupole-ACSM (Ng et al., 2011) for a time resolution of 30 min. The instrument
338 measures the mass and chemical composition of non-refractory submicron aerosol particles – i.e., organic substances, nitrates,
339 sulphates, ammonium, and chloride – thus generating an invaluable database for the research community to characterise the
340 particulate sources and evolution. The operational principle of the instrument is briefly described in the following: the aerosol
341 enters the inlet where the aerodynamic lens efficiently samples and focuses submicron particles to the subsequent vacuum
342 chamber; here, the particles impact on a resistively heated porous tungsten surface at approximately 600°C which vaporises
343 the non-refractory particulate; the vaporised matter is subsequently ionised by electronic impact and detected through the ToF
344 analyzer. In this case, the 24-inch Nafion dryer installed upstream the instrument eliminates the complicating inlet effects due
345 to particle composition dependent water uptake (Middlebrook et al., 2012).

346 ACSM was installed in February 2023 and worked for some months in almost continuous way. Then some interventions were
347 requested to accomplishing the optimization requests from ACTRIS aerosol in situ Central Facility, and the ACSM restarted
348 operations just recently in April 2024. Anyhow the 3 months of almost continuous measurements performed in 2023 already
349 provide some insights about aerosol particles present at the surface in Potenza. Fig. 8 reports daily concentrations for the 4
350 components as measured by ACMS in February-March-April 2023 period. Median values are preferred to mean ones for
351 avoiding the strong influence of outliers and spikes in the reported values. Monthly pie charts show the relevance of the
352 difference components for each one of the 3 months. As a general comment, we could say that the Potenza site exhibits low
353 PM concentrations and a very high contribution of the organic substances, as observed in rural areas (see for comparison as
354 example Atabakhsh1 et al., 2023 and Zhao et al., 2020). The observed peaks in the total concentration but more pronounced
355 in the organic component could be related to tree pollen events typically occurring in such period.

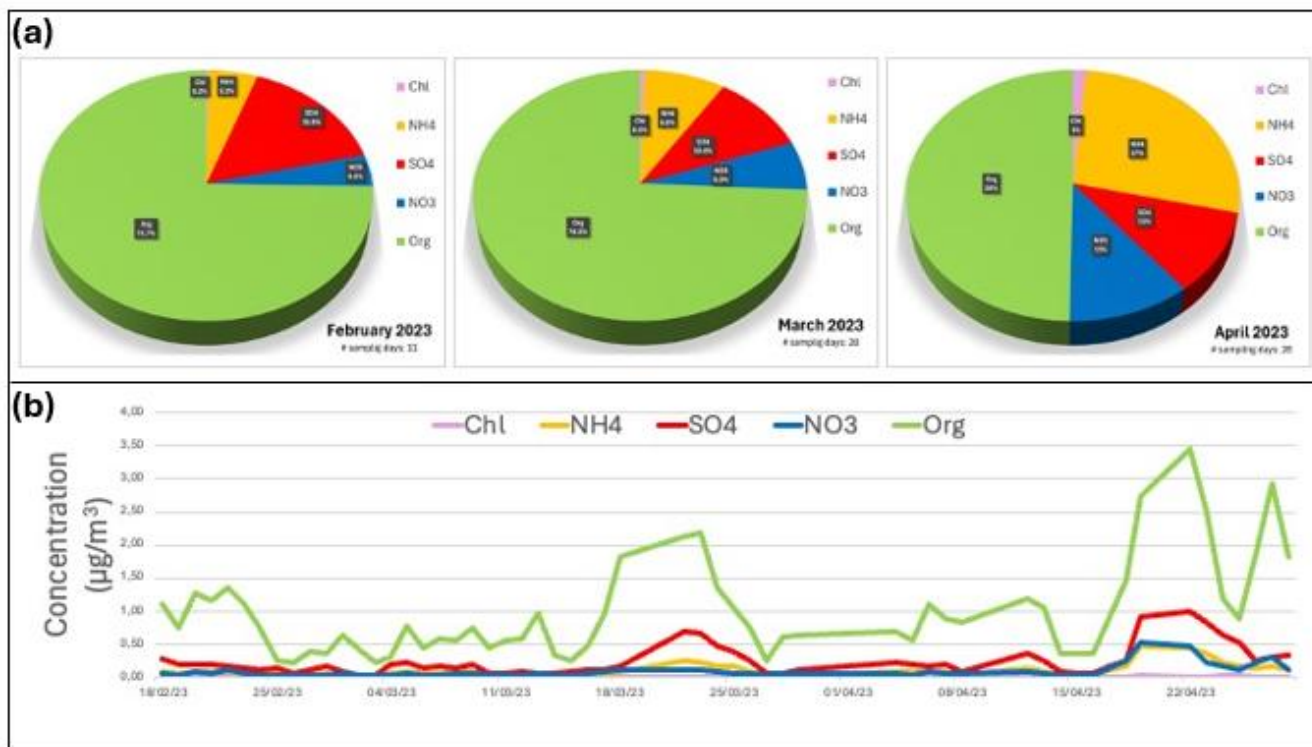


Figure 8: Daily medians of the mass fraction (a) and mass concentration (b) of each of the 4 chemical components of non-refractory submicron aerosol particles observed at CIAO in February – March – April 2023.

4.4 PMx samplers and PMx monitor

Additionally to the online instruments report above, the field laboratory is equipped with two PMx samplers for the continuous sampling and concentration measurement of PM₁₀, PM_{2.5} and PM₁ (aerosol particles with an aerodynamic diameter less than 1 μm) mass fractions collected over both Teflon and quartz filters; the determination of the mass of collected samples is based on the β -ray attenuation equivalent method, which strongly reduces the workload and the operator-associated variability if compared to the standard gravimetric method (Baltensperger et al., 2001). In particular, the device measures the attenuation of β -ray across the filter medium which collects particulate matter, and the attenuation of intensity in β -ray is proportional to the amount of material present. Each PMx sampler is equipped with two independent sampling lines (i.e., PM₁₀/PM_{2.5} and PM_{2.5}/PM₁), thus enabling the simultaneous collection of different PM fractions on independent filters. According to the workflow reported in Fig. 4, the particulate collected over the filters is subjected to further analysis within the chemical laboratory: the PM₁₀, PM_{2.5} and PM₁ collected over 24h on Teflon filters are analysed to determine the concentration of metals

by means of the ICP-OES. On the other hand, the PM_{2.5} collected over 24h on quartz fibre filters are analysed to quantify the organic carbon (OC) and elemental carbon (EC) fractions using the thermal optical method by the OC/EC analyzer; the utilisation of quartz fibre filters for the OC/EC analysis is strictly recommended by the WMO/GAW 2016 guidelines, and it constitutes the only exception to the Teflon filters commonly used for other analyses. In fact, the particulate collected on Teflon filters is not limited to ICP-OES analysis but can also be analyzed through alternative techniques such as X-ray fluorescence (XRF) and Particle Induced X-ray Emission (PIXE) in order to find complementarities between the three techniques for the determination of a range of metals.

Furthermore, even if not included in the mandatory ACTRIS variables to be measured, the mass concentration for the cut-off diameters of PM₁₀, PM_{2.5} and PM₁ belongs to the set of standard measurements to monitor the particulate matter, providing insight into the separation of fine and coarse particles within the aerosol.

The PMx monitor operating at CIAO currently represents one of the main automated measurement systems for studying the concentration levels of particulate matter in ambient air. Based on the detection principle of the light scattering at the level of single particles, the system offers simultaneous real-time measurements of PM₁₀, PM_{2.5} and PM₁ and particle number distribution with a resolution of 0.1 µg m⁻³.

4.5 Chemical laboratory

The CIAO chemical laboratory is equipped with an ICP-OES and an OC/EC analyzer. The ICP-OES is used to determine the qualitative and quantitative elemental composition of the metals present in the atmospheric particulate with high sensitivity, at values below the 1 µg l⁻¹ limit for certain elements. The metals are introduced into the atmosphere from various anthropogenic and natural sources. Anthropogenic metals are released into the atmosphere during combustion of fossil fuels and wood, as well as during high temperature industrial processes and waste incineration; natural emissions result from a variety of processes acting on crustal minerals, including volcanism, erosion, surface winds, forest fires and ocean evaporation (Allen et al., 2001; Pakkanen et al., 2001; Rajšić et al., 2008). Various metals are used as marker for the identification of emission sources: aluminium and silicon are primarily derived from soil and rocks (crustal elements); sodium and chlorine are typically associated to marine aerosol particles; arsenic, cadmium, manganese and lead mostly derive from combustion of fossil fuels occurring at high temperature, to name a few. The ICP-OES analysis of particulate matter requires a preliminary microwave digestion of the filter in acidic conditions to extract the metals, carried out by means of a microwave digester (ETHOS UP, FKV). The obtained liquid sample is then nebulized and introduced into the plasma as an aerosol suspended in the argon gas: due to the high temperatures within the plasma (7000 – 10000 K), a significant fraction of most elements exists as atoms or ions in the excited state, causing an intense polychromatic emission which continuously brings back the elements to their ground state. The polychromatic emitted light is dispersed into individual wavelengths by a polychromator and detected

by a photosensitive charge-coupled device (CCD). The concentration of each metal in the sample is obtained by using a calibration curve referred to a solution containing the analysed elements of known concentration.

The multi-wavelength OC/EC analyzer compliant with ACTRIS is used to quantify the total carbonaceous content of the particulate matter (total carbon, TC) and the OC and EC subfractions. EC is essentially a primary pollutant, emitted directly from the incomplete combustion of fossil fuels and the pyrolysis of biological material during combustion, whereas OC can be directly emitted from the incomplete combustion of organic materials and the degradation of carbon containing products such as vegetation – primary OC – or produced from atmospheric reactions, involving gaseous organic precursors, i.e., secondary OC (Zhou et al., 2006). The operational principle of the thermal/optical analysis is based on the preferential desorption of OC and EC materials under different temperatures and atmospheres programmed within specific thermal protocol, such as the EUSAAR_2 (Cavalli et al., 2010) which is currently used within the ACTRIS community. OC usually desorbs under a non-oxidising helium atmosphere at temperatures up to 570°C, while the EC is combusted in an oxidising atmosphere with 2% O₂ at temperatures up to 850°C. However, since part of the OC turns into the light-absorbing pyrolytic carbon which desorbs during the oxidising mode, the correct discrimination between the OC and the EC fractions is conveniently identified with the point at which the light transmission reaches the pre-pyrolysis value. The liberated carbon is then completely oxidised to carbon dioxide passing through a heated catalyst MnO₂ and finally quantified by an NDIR (Non-Dispersive Infrared) detector.

416

417 **5 Combined deployment of aerosol remote sensing and in-situ measurements**

Combined approaches using aerosol particles profiling and in-situ measurements are one of the most beneficial strategies in aerosol research, allowing an accurate typing and estimation of the impacts of particulate matter (Molero et al., 2020). Remote sensing techniques provide the vertical profile of the particle size distribution of the aerosol particles as well as further physical and optical properties useful for understanding complex atmospheric phenomena (Vratolis et al., 2020); however, they are not able to provide information under cloudy sky conditions or at the ground level, where the identification of aerosol particles type is only possible using the in-situ instrumentation. The in-depth typing of the aerosol particles require the information on the chemical composition, attainable only by means of in-situ measurements. The complete set of data resulting from the combined approaches is crucial for identifying the sources and the evolution of concentration levels of particulate matter over time (Bressi et al., 2021), and it is of paramount importance for the implementation of controls or policies to reduce aerosols that negatively affect air quality and public health.

The complete picture of the aerosol particles-typing is also expected to clarify further the climate effects of particulate matter. In fact, the estimation of the radiative effect of atmospheric aerosol particles requires the knowledge of multiple parameters,

including the aerosol concentration, the optical properties, the chemical composition, the presence of clouds and the albedo of the underlying surface. The accurate identification of aerosol particle types is also needed to improve the understanding of atmospheric dynamics and long-range transport, to improve satellite aerosol retrieval algorithms, and to validate climate models.

The multiwavelength polarisation Raman lidar is a well-established active remote sensing technique for the detection and characterization of aerosol-types (Nicolae et al., 2018; Papagiannopoulos et al., 2018). Specifically, it can provide vertically resolved information on extensive (e.g., aerosol backscatter coefficient, aerosol extinction coefficient and volume depolarization ratio) and intensive (e.g., Ångström exponent, lidar ratio and particle depolarization ratio) aerosol optical properties. The extensive properties depend on the aerosol particles concentration, whilst intensive ones are type-sensitive providing indication about the particle size, shape, and indices of refraction that allow for the characterization of different aerosol types. Nevertheless, the intensive properties might not be sufficient to guarantee accurate typing, as some aerosol types (e.g., volcanic and desert dust particles) have very similar intensive properties but are attributed to different sources and generating mechanisms. For this reason, the discrimination of aerosol particles that typically have the same optical characteristics calls for the combined use of lidar observations and transport model simulations. The aerosol in-situ observations can help in the assessment of the uncertainty of remote sensing-retrieved products like mass concentration, refractive index and fine-particle concentration obtained through inversion algorithms (e.g., Veselovskii et al., 2012; Lopatin et al., 2013).

Furthermore, the availability of collocated in situ and remote sensing measurements of aerosols also represents an added value for modelling. Indeed, it can contribute to the increase in the accuracy of model predictions, allowing the reduction of the uncertainty of aerosol measurements in the atmosphere (e.g., Vratolis et al., 2020), as well as to a better evaluation of aerosol models. In recent years, collocated datasets have also been increasingly utilized for training machine learning-based models, as demonstrated by Redemann and Gao (2024). To emphasize the potential synergy and added value of combining in-situ and remote sensing techniques, Table 2 presents a comprehensive list of instruments and the respective parameters they measure.

	Instruments	Parameters
Cloud Remote Sensing	Ka-band Doppler radar Metek MIRA-35	Vertical profiles of Doppler spectrum moments (e.g. Signal-to-noise ratio, Doppler velocity, spectral width, equivalent reflectivity factor) and of linear depolarization ratio of atmospheric targets (clouds, precipitations, insects, giant aerosols). Typical measurement range: 100m-15km
	Compact Ka-band Doppler radar MIRA 35C	Same as above. Typical measurement range: 100m-12km ssss
	W-band Doppler radar RPG-FMCW-94	Same as above. Typical measurement range: 50m-12km
	K-band Doppler radar Metek MRR-PRO	Vertical profiles of hydrometeors' Doppler spectrum moments, of raindrop size distribution, liquid water mass concentration and rain rate. Typical measurement range: 15m-6km
	Microwave radiometer RPG-HATPRO-G5	Vertical profiles of temperature, humidity and cloud liquid water mass concentration; integrated precipitable water vapor and cloud liquid water path. Typical measurement range: 0-10km
	Ceilometer Vaisala CL51	Vertical profiles of attenuated backscatter coefficient from atmospheric particles (aerosols, clouds and precipitations), cloud base heights, aerosol vertical layering. Typical measurement range: from near surface (15m) up to 12km for clouds and depending on the aerosol load in a cloud-free atmosphere.
	Ceilometer Vaisala CL31	Same as above. Typical measurement range: from near surface (15m) up to 8km for clouds and depending on the aerosol load in a cloud-free atmosphere.
	Ceilometer Lufft CHM15k	Same as above. Typical measurement range: from near surface (15m) up to 15km for clouds and depending on the aerosol load in a cloud-free atmosphere.
	2 Doppler lidars Halo Photonics Stream LineXR	Vertical profiles of attenuated backscatter coefficient from atmospheric particles (aerosols, clouds and precipitations) and of vertical/horizontal wind components.

Trace gases Remote Sensing	FTIR Bruker 125HR	Infrared spectrum contain the signatures of vibrational-rotational transitions of numerous trace gases in the terrestrial atmosphere as they absorb solar radiation (O ₃ , HCl, HF, ClONO ₂ , HNO ₃ , N ₂ O, CH ₄ , CO, C ₂ H ₆ , and HCN)..
Aerosol Remote Sensing	Fixed multi-wavelength Raman lidar	Aerosol extinction coefficients at 355 and 532 nm; Aerosol backscatter, Volume and particle depolarization ratio at 355, 532 and 1064 nm and water vapour mixing ratio
	Mobile multi-wavelength Raman lidar	Aerosol extinction coefficients at 355 and 532 nm; Aerosol backscatter, Volume and particle depolarization ratio at 355, 532 and 1064 nm
	MUSA Transportable Fixed multi-wavelength Raman lidar	Aerosol backscatter at 355, 532 and 1064, Aerosol extinction coefficients at 355 and 532 nm, Volume and particle depolarization ratio at 532
	Scanning UV Raman lidar	Aerosol backscatter, Aerosol extinction coefficients, Volume and particle depolarization ratio at 355
	Automatic sun/sky/lunar photometer Cimel 318T	Aerosol Optical Depth (AOD), Volume Size Distribution (VSD), complex refractive index (n), shape factor, water vapor content.

Aerosol in-situ	SMPS	Size distribution and concentration of the particles in the size range 10 – 800 nm
	APS	Size distribution and concentration of the particles in the size range 0,8 – 10 µm
	CPC	Concentration of the number of particles with dimensions > 10nm
	Nephelometer	Aerosol scattering and backscattering coefficients at 450, 525 and 635 nm
	Aethalometer	Aerosol absorption coefficients and BC concentration at seven wavelengths in the range of 370-950 nm
	PM _x Monitor	Mass concentration for the cut-off diameters of PM ₁₀ , PM _{2.5} and PM ₁
	ACSM	Real-time chemical characterization of the main organic and inorganic components of the non-refractory sub-micrometric aerosol particles
	ICP-OES	Qualitative and quantitative elemental composition of the metals on collected filters of aerosol particles
	OC/EC Analyzer	TC and subfraction OC/EC concentrations on collected filters of aerosol particles

Table 2: List of all CIAO remote sensing and in-situ instruments and respective parameters.

In the following subsections we present three emblematic cases recurring at CIAO where the combined deployment of the in-situ and remote sensing observations is expected to be of added value: 1) Wildfires become more and more relevant in the Mediterranean, especially in view of the changing climate that is expected to increase temperature and in turn will affect their frequency, duration and intensity in the next decades. In this context, small and local fires are widely distributed, and their characteristics and assessment could be important at global level. De Rosa et al. (2022) showed with the use of lidar observations that fresh fires can be surprisingly characterised by low absorption; this would imply a different impact of local fires in the radiation budget which requires investigation and validation by means of in-situ measurements. 2) Local pollution during winter and adverse weather can be investigated in a more exhaustive manner only by in-situ observations, since lidar observations provide very little information due to the generally low and unresolved by lidars PBL height. 3) Desert dust intrusions often reach Europe and especially the Mediterranean Basin affecting local air quality, health and ecosystem and

socio-economic sectors (e.g., Monteiro et al., 2022). Given all the above, the deployment of in-situ measurements at well-equipped sites like CIAO is crucial to quantify the impact at the ground level.

5.1 Local wildfires

The study of smokes from wildfires spreading over short distance represents a great example for a synergistic approach based on remote-sensing and in-situ techniques. In such a case, the smoke particles spread mainly at low levels and deposit fast on the ground, where in-situ measurements are the only tool to provide reliable information to support and integrate what is observed above medium overlap region, a prerogative of remote-sensing techniques.

The multiwavelength polarisation Raman lidar is a well-known tool to study smoke layers in the atmosphere, being able to separate aerosols according to their specific optical signature (Ohneiser et al., 2021). Specifically, a sign of the dominance of smoke in the aerosol layer is the aerosol extinction-to-backscatter ratio (the so-called lidar ratio, S) at 532 and 355 nm, which is typically high (i.e., > 50 sr) as a consequence of the presence of absorbing BC produced during the biomass burning; moreover, the ratio of S measured at the different wavelengths may be used as an indicator of the phase of the ongoing wildfire (e.g., Nicolae et al., 2013). Other lidar parameters largely used to investigate the smoke are the particle linear depolarization ratio (PLDR) and the Ångström exponent (AE), which provide information about the shape and the size of the particles, respectively. In the case of a local wildfire, the observation of quasi-spherical and relatively small particles is expected, since the newly produced smoke particles do not have the time to undergo modifications during transport.

The Ångström absorption and scattering exponents (AAE and SAE) - derived from the aethalometer and nephelometer measurements, respectively - provide the optical typing of the smoke, with the value of AAE expected to correlate with the lidar observations (Cazorla et al., 2013) and, therefore, to the nature of spreading fire.

Among the aerosol in-situ instruments, the aethalometer is crucial to study smokes produced during wildfires, being able to quantify the BC originated from the incomplete combustion of carbonaceous matter and providing an estimate of the biomass burning (BB) apportionment to the overall BC (Sandradowi et al., 2008). Additionally, the OC/EC thermal/optical analysis on $PM_{2.5}$ fraction is very important because the increase of organic carbon and elemental carbon concentrations has been the most indicated as an element that reflects wildfire emissions. Fine particles ($\leq 2.5 \mu m$) are a major pollutant from wildfire smoke. Key in-situ analyses include size distribution and concentration measurements using SMPS and CPC, as fine particles are more abundant during fires compared to other periods. Real-time PM_x monitoring confirms increases in $PM_{2.5}/PM_{10}$ and $PM_1/PM_{2.5}$ ratios during fire events. Finally, the in-situ investigation of wildfire smoke is completed by the chemical analysis obtained with the ToF-ACSM: in particular, key tracers of biomass burning organic aerosol particles in mass spectra are the enhanced signals at m/z 60 and 73 attributed to $C_2H_4O_2^+$ and $C_3H_5O_2^+$ ions, respectively, coming from the fragmentation of the so-called “levoglucosan-like” species originated from the pyrolysis of cellulose (Cubison et al., 2011). Finally, the chemical analysis of

the filters through the ICP-OES is fundamental for tracking the levels of potentially toxic elements (PTEs) such as As, Sb, Cd, Hg, Pb, Cr, Cu, Ni, Se, Tl, Sn, V, and Zn. This monitoring is vital as these elements have the potential to be released into the environment during wildfires, posing a threat to humans and animals when their absorbed doses surpass the established reference values (Pacifico et al., 2023).

This case underlines the critical need for a combined approach, where in-situ measurements bridge the gap and enhance the interpretation of remote-sensing data, showcasing the strength of CIAO's integrated monitoring capabilities.

5.2 Local pollution in wintertime

Winter months commonly exhibit heightened air pollution levels, primarily attributed to temperature inversions. Inversion occurrences involve a layer of warm air confining colder air and pollutants close to the ground, impeding their dispersion into the atmosphere. Unlike summer air pollution, winter conditions result in the prolonged presence of pollutants, increasing the likelihood of higher inhalation rates. This extended exposure raises health concerns for individuals, as reduced ventilation and dispersion contribute to potential health effects.

Air quality near the ground during winter is expected to be dominated by local residential heating emissions with the contribution of vehicle engine exhausts. For this season, the in-situ measurements represent the most viable way to investigate the aerosol particles distribution and composition, while the deployment of remote sensing instruments (e.g., lidar) is limited by instrumental and environmental factors. During wintertime, the condensation of water droplets (especially during nighttime) along with the recurrent formation of cloud layers attenuate the laser beam, thus impeding the lidar retrievals; moreover, even under clear sky conditions, the particulate is usually confined within the first 300 m from the ground (i.e., the typical PBL layer thickness in wintertime), where the active remote sensing techniques are not able to provide reliable results, because of the typically overlap between laser beam and receiving system in lidar at this vertical range .

The climatological profile of aerosol backscatter at 532 nm for winter season 2000-2019 at CIAO (blue line in Fig. 9) shows very clean air respect to other seasons in the whole investigated atmospheric column (https://doi.org/10.57837/cnr-ima/ares/actris-earlinet/level3/climatological/2000_2019/pot).

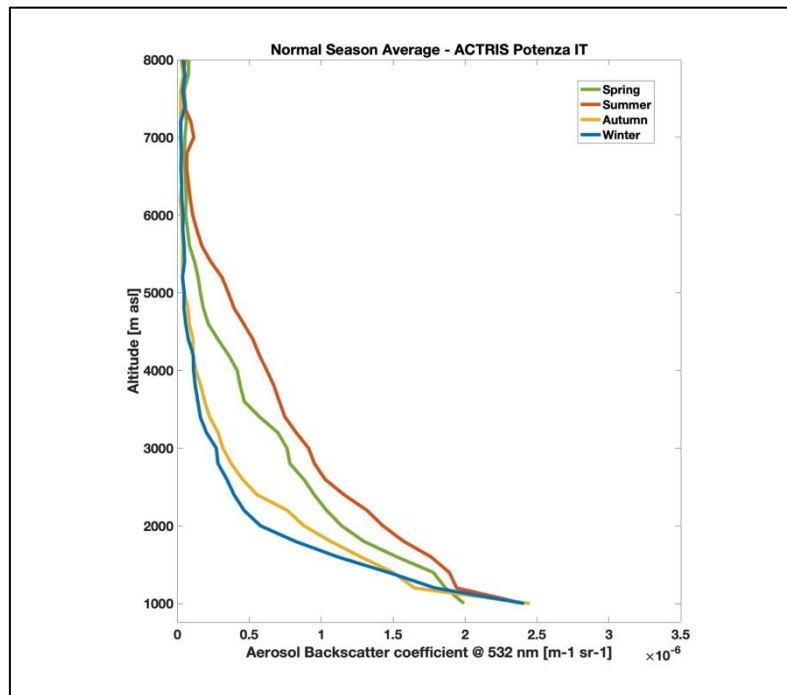


Figure 9: Climatological profiles of the aerosol backscatter at 532 nm observed at CIAO from 2000 to 2019. Normal Season average is reported: each profile is the average of all aerosol backscatter profiles observed at CIAO for each season in routinely measurements collected from 2000 to 2019.

Only the last point close to the surface is slightly higher respect to the other seasons, but the information content is too low for further investigation. These cases are typically considered as clean day from the aerosol remote sensing perspective. However, it must be noted that lidar is blind to the lowest portion of the atmosphere, where pollutants are concentrated due to the low boundary layer height (PBL).

On the other hand, only the in-situ measurements, which do not see above the boundary layer height, can well capture what's happening close the surface.

In this context, we investigate the average daily concentration of elemental carbon (eBC) obtained by the aethalometer (Figure 8a), covering the period from June 2023 to April 2024, to have a first insights into air quality near the ground during winter. Our analysis reveals no significant increase in eBC concentration during the winter months compared to background levels observed in summer. However, when examining the daily average percentage of black carbon (BC) originating from biomass burning (BB%), as determined by the Sandradewi model (Sandradewi et al., 2008), in conjunction with the daily average temperature data obtained from the Vaisala AWS310 weather station situated at the site (Figure 8b), an intriguing trend

emerges. It becomes evident that BB% is substantially higher during winter months than during summer months. Given the minimal occurrence of wildfires and prescribed burns at the site during winter, the primary source of biomass burning influence can be attributed to residential burning, a consequence of the notably low temperatures experienced during that period.

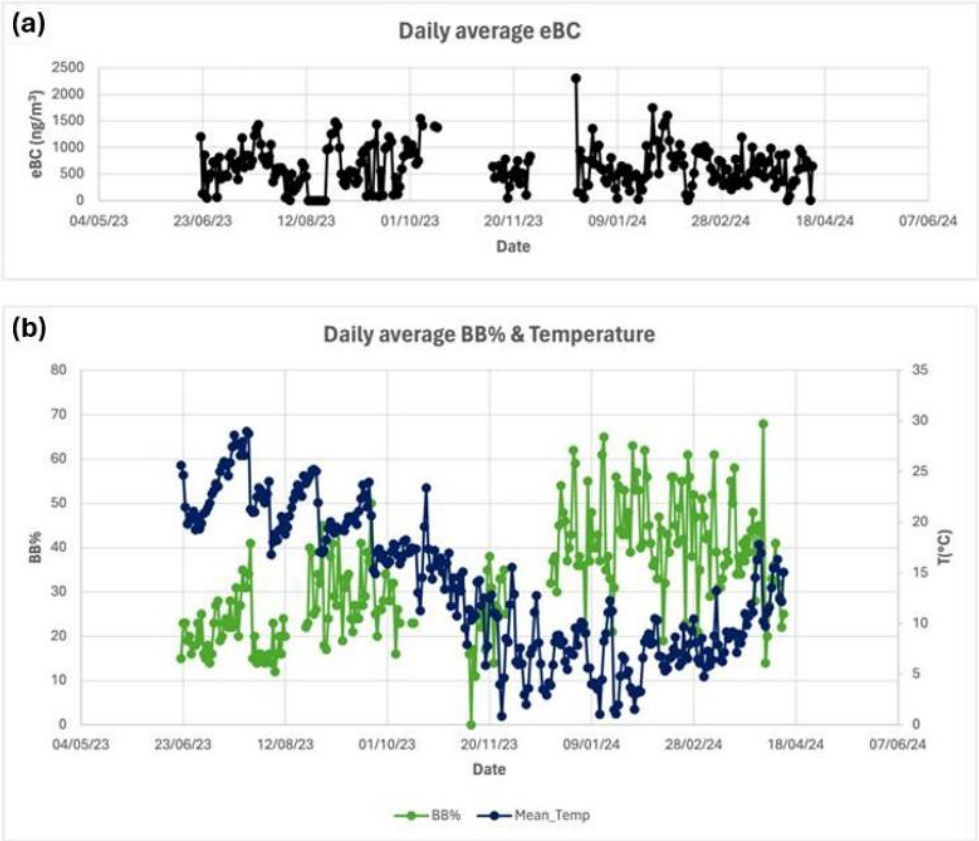


Figure 8: Daily average eBC concentration obtained by aethalometer from June 2023 to April 2024 a); daily average BB% determined by the Sandradewi model and daily average temperature data obtained from the Vaisala AWS310 weather station from June 2023 to April 2024 b).

These first data indicate that the main source of BC during winter at our site is predominantly from local residential heating emissions. Unlike remote sensing, which may suggest clean air conditions, in-situ measurements reveal significant pollution at ground level, underscoring that winter cases should not be considered background conditions in the boundary layer region. Therefore, this preliminary study demonstrates that combining remote sensing and in-situ measurements provides critical insights that neither method can achieve independently. Future studies could expand on this by incorporating additional in-situ instruments alongside the aethalometer.

For example, OC/EC analysis on the PM_{2.5} fraction could support and complement aethalometer results (Schmidl et al., 2008; Gonçalves et al., 2010; Pio et al., 2011; Sirignano et al., 2019), while a nephelometer could provide ground-level optical parameters, such as the scattering coefficient (σ_{sp}) and backscattering coefficient (σ_{bsp}), which are linked to particle concentrations, particularly fine and ultrafine particles typical of heating emissions (Esteve et al., 2012). The ToF-ACSM could offer a detailed chemical composition of PM₁, expected to reveal a dominance of organic matter from combustion processes. Secondary ammonium nitrate (NH₄NO₃), associated with residential wood burning and diesel emissions (via NO_x), could also explain exceedances in fine particle fractions during winter (Chen et al., 2012). Finally, filter analysis with ICP-OES could identify metals in the particulate matter (e.g., Na, Mg, Zn, Pb) originating from specific sources such as fossil fuel and biomass combustion, vehicular traffic, and dust resuspension (Dušan et al., 2017; Zhi et al., 2021). This in-situ multi-instrument approach would provide a comprehensive view of particulate composition and sources during winter pollution episodes at the surface, enabling a deeper insight into winter aerosol conditions, addressing air quality challenges, and accurately evaluating their health impacts.

5.3 Dust intrusions

During summer and spring, the site is regularly affected by Saharan dust intrusions (Mona et al., 2006). Desert dust particles have many effects: they can impact climate, the precipitation cycle, and human health (Sokolik et al., 2007; Mona et al., 2023). Mineral dust particles can act as cloud condensation nuclei (CCN) and thereby determine the concentration of the initial droplets, albedo, precipitation formation, and lifetime of clouds (Levin et al., 1996; Levin et al., 2005). The multiwavelength polarisation Raman lidar provides highly resolved spatial and temporal atmospheric profiles that allow for the separation of the different aerosol layers (Pappalardo et al., 2004b; Papagiannopoulos et al., 2018). Large and irregular shaped Saharan desert dust particles produce medium lidar ratios S, relatively high PLDR values and they are spectrally neutral to backscatter and extinction producing low Ångström exponent referred to the wavelengths 355-532 nm (Freudenthaler et al., 2006; Fernandez et al., 2019). In fact, mineral desert dust aerosol particles predominantly consist of coarse mode particles of irregular shapes (Mahowald et al., 2014). In-situ measurements, in case of sedimentation events, provide complementary information on the advected dust. Low values of nephelometer-derived SAE that indicate coarse particles and, conversely, high aethalometer-derived AAE values that demonstrate the wavelength dependent absorption (Cazorla et al., 2013). During dust-dominated atmospheric conditions, sedimentation increases, returning large particles to the ground. The APS size distribution measurements of coarse particles are crucial for dust studies. A low PM_{2.5}/PM₁₀ ratio from real-time PM_x monitor data confirms the dominance of the coarse fraction during desert dust events. Additionally, 24-hour PM₁₀ mass concentrations

578 measured by the PM_x sampler (SWAM 5a-Dual Channel Monitors, FAI Instruments) are higher during dust events, often
579 exceeding the European daily limit (2008/50/CE European directive).

580 For chemical characterization, ICP-OES detects the mineral fraction's elemental composition, particularly crustal elements
581 like Al, Ca, Fe, K, and Na, along with Rare Earth Elements (REEs). These concentrations are significantly elevated during
582 dust events compared to annual averages (Aydin et al., 2012; Rodriguez-Navarro et al., 2018; Mărmureanu et al., 2019).

583 In the following we report an example of aerosol remote sensing and in-situ observation for a Saharan dust intrusion at CIAO
584 to demonstrate the possibilities for complementary combination of data from lidar and in-situ aerosol measurements. Even if
585 only the APS instrument was available at that time, the presence of just one in-situ instrumentation already shown the
586 importance of such combination of techniques. The observations are related to the second half of June. Figure 9a reports the
587 fine mode fraction as retrieved from CIAO photometer measurements and available at aeronet.gsfc.nasa.gov. This parameter
588 provides information about the fraction of fine mode particles respect to the coarse one as obtained from the AOD (Aerosol
589 optical Depth) measurements. This parameter is retrieved from columnar measurements and therefore refer to the total
590 atmospheric column. Fig 9a clearly shows that in the 20-23 June period the coarse particles are more abundant respect to
591 previous and following period. For the same period Hybrid Single-Particle Lagrangian Integrated Trajectory (HYSPLIT)
592 backward trajectories ending over Potenza indicate Sahara desert as potential source of the observed particles.

593 Lidar observations provide a better insight of the temporal and vertical distribution of the aerosol particles at CIAO on those
594 days. Figure 9b-c report available Lidar observations for the period. It shows the color-maps of the vertical distribution and
595 temporal dynamics of the aerosol as time series of range-corrected lidar signals at 532 nm for the night of 22 June 2023 and
596 the daytime day of 23 June 2023. In particular, these plots report the component of backscattered signals at 532 cross-polarized
597 respect to the emitted laser light: the presence of high cross-polarized backscatter signals is a signature of presence in that
598 portion of 4d atmospheric region of aspherical particles, like Saharan dust ones.

599 The representation of the aerosol particles distribution during the night of 22 June (Fig. 9b) shows two main layers of dust:
600 one at an altitude close to 1 km above ground level (agl) and a second denser one above it at a height of approximately 3 km
601 agl. Particularly interesting for the potential link with in-situ measurements is a branch of the lower layer around 01:30 in the
602 night between 22 and 23 June, which seems to descent in altitude and could potentially sediment at the ground. It is worth to
603 note that the lidar blind region for the instrument available at the time of the measurements was around 400 m not allowing to
604 further investigate this point. Over the next day (Fig. 9c), the color-map again indicates the presence of dust from 9:00 to 12:00
605 at similar heights to 22 June but with lower density until it disappears after 12:00.

606

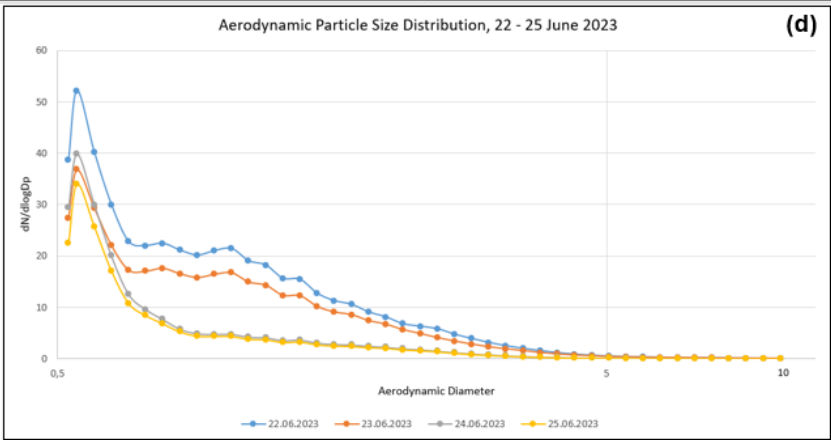
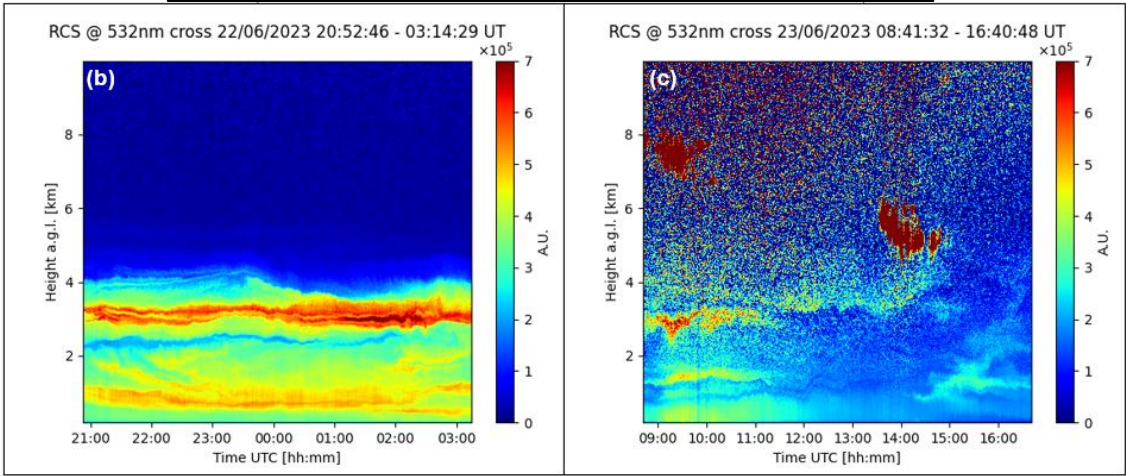
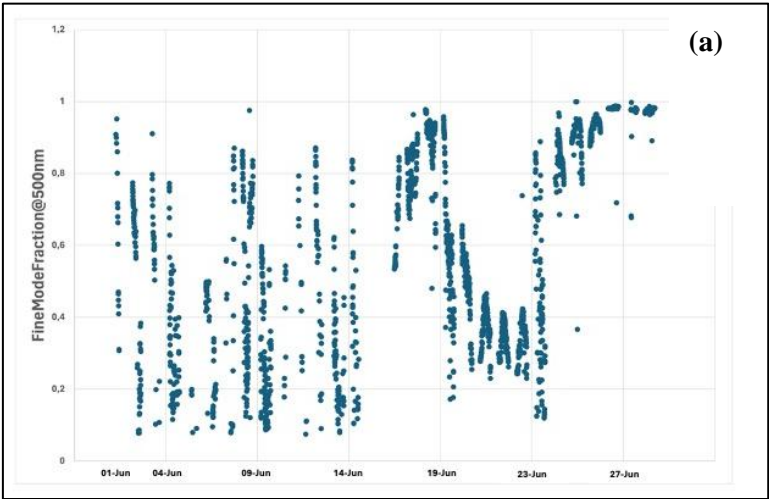


Figure 9: Fine mode fraction as retrieved from CIAO photometer measurements related to the second half of June (a), color-coded time series of range-corrected lidar signals measured at 532 nm cross-polarized channel obtained with the MUSA lidar system on 22 June 2023 (b) and 23 June 2023 (c), aerodynamic particle size distribution daily averages obtained with APS on 22-25 June 2023 (d).

Online observations at the ground allow a better understanding of the dust presence at the surface exploring also the status after the 22-23 June. In that period, only APS and aethalometer were operational at CIAO.

Fig. 7d shows the aerodynamic particle size distribution daily averages obtained with APS on 22-25 June 2023 and provides complementary information to that obtained through lidar and photometer measurements. Indeed, Fig 7d distinctly illustrates that there is negligible variance in the concentration of ultrafine particulates between dust (22-23 June) and non-dust (24-25 June) days, instead there is a noticeable rise in the concentration of fine and coarse particles with a diameter of up to 5 μm on the dust days (22-23 June) compared to the non-dust days (24- 25 June); demonstrating how during dust events the atmosphere is dominated by large particles (Fig 7a) distributed over different altitude ranges (Fig 7b-c) and if sedimentation is favoured, this leads to a greater return to ground level in the coarse mode (Fig. 7d).

This case demonstrates strong agreement between remote sensing and in-situ measurements in identifying and characterizing a desert dust event. Lidar provides detailed vertical and temporal distribution of aerosols, while in-situ measurements capture surface-level dynamics, overcoming lidar's limitations in the blind region near the ground. Together, these methods reveal a more complete picture of the dust event.

Future synergistic products could involve integrating additional in-situ instruments with remote sensing to provide richer data for events like this. For example, upgraded systems at CIAO, including advanced offline and online instruments, will enable deeper analyses of similar phenomena. While a detailed investigation of this event is beyond the scope of this paper, it sets the foundation for future studies exploring the full potential of these complementary approaches.

6 Conclusions

The recent upgrade of the CIAO observatory with aerosol in-situ laboratory in addition to the well-established remote sensing instrumentation significantly enhances its observational capacity. The integration of in-situ and remote sensing measurements offers a more complete understanding of aerosol behaviour, enabling detailed studies from ground level up to the stratosphere. This combination adds value by providing both vertical profiles by remote sensing measurements and precise ground-level chemical and physical properties through in-situ measurements, which is crucial for improving climate models and understanding aerosol impacts on human health.

Establishing the aerosol in-situ facility has been a complex and labour-intensive endeavour. The process, which began in 2018, required careful planning, technical expertise, and collaboration with field specialists. The setup involved designing and

643 implementing ACTRIS-compliant inlets, sampling lines, and advanced instruments to ensure accurate and reliable
644 measurements. This development highlights the significant effort required to meet international standards and provide high-
645 quality data for the scientific community.

646 Given CIAO's strategic location in the Mediterranean, the case studies planned for future research are especially relevant. The
647 site is frequently affected by Saharan dust intrusions, which impact air quality and ecosystems, and the observatory is
648 strategically positioned to study these phenomena. Moreover, the Mediterranean is also prone to wildfires, which are projected
649 to increase in intensity and frequency due to climate change. The CIAO observatory can monitor both the short-range transport
650 of smoke from local fires and long-range plumes from major events, providing insights into their effects on air quality and
651 human health. Lastly, local winter pollution, which results from residential heating, can also be analysed in detail, particularly
652 during temperature inversions that trap pollutants near the ground. The combination of in-situ and remote sensing
653 measurements will help investigate these key environmental issues.

654 Furthermore, the next-to-come ICOS Atmospheric Class 1 site at CIAO (first step of labelled process already passed) will
655 offer other possibilities of synergistic studies and integration among RIs in the environmental field. In this direction, CIAO is
656 deeply involved in the developments of ITINERIS (Italian Integrated Environmental Research Infrastructures System), an
657 overarching National project for enhancing the interlinkages of all the Italian RIs in the environmental domain. The multi-
658 platform and multi-disciplinary approach of the observatory coupled with the open data and open access philosophy is key for
659 better addressing complex atmospheric and environmental questions posed by climate change and anthropization processes.

660

661 **Appendix A**

662 **Glossary of acronyms**

663 AAE: Ångström absorption exponent

664 ACTRIS: (Aerosol Clouds and Trace gases Research InfraStructure)

665 AE: Ångström exponent

666 AERONET: Aerosol Robotic NETwork

667 APS: Aerodynamic Particle Sizer

668 BB: Biomass Burning

669 BC: Black Carbon

670 CCD: Charge Coupled Plasma

671 CIAO: (CNR-IMAA (Consiglio Nazionale delle Ricerche-Istituto di Metodologie per l'Analisi Ambientale) Atmospheric
672 Observatory)

673 CNN: Cloud Condensation Nuclei

674 CPC: Condensation Particle Counter
675 DMA: Differential Mobility Analyzer
676 EARLINET: European Aerosol Research Lidar Network to Establish an Aerosol Climatology
677 eBC: equivalent Black Carbon
678 EC: Elemental Carbon
679 FTIR: Fourier Transform Infrared Spectroscopy
680 Galion: GAW Aerosol Lidar Observation Network
681 GAW: Global Atmosphere Watch
682 GCOS: Global Climate Observing System
683 GRUAN: GCOS Reference Upper-Air Network
684 HYSPLIT: Hybrid Single-Particle Lagrangian Integrated Trajectory
685 ICOS: Integrated Carbon Observing System
686 ICP-OES: Inductively Coupled Plasma Emission Spectrophotometer
687 NDIR: Non-Dispersive Infrared
688 OC: Organic Carbon
689 PBL: Planetary Boundary Layer
690 PIXE: Particle Induced X-ray Emission
691 PLDR: Particle Linear Depolarization Ratio
692 PM: Particulate Matter
693 RH: Relative Humidity
694 RI: Research Infrastructures
695 SAE: Ångström scattering exponent
696 SMEs: small and medium-sized enterprises
697 SMPS: Scanning Mobility Particle Sizer
698 TC: Total Carbon
699 ToF-ACSM: Time of Flight Aerosol Chemical Speciation Monitor
700 WMO: World Meteorological Organization
701 XRF: X-ray Fluorescence

702

703 **Author contributions**

704

TL, AM and ST contributed to writing – original draft preparation. TL, AM, ST, CCol and MM contributed to visualization. TL, AM, ST, FC, DA contributed to methodology. TL and MM contributed to formal analysis. DA, AG, CD, ER and CC contributed to resources. CCor, SG, RMAP, GP contributed to funding acquisition. EL contributed to software. TL, AM, ST, AA, BDR, MR, LM contributed to writing - review & editing. FC, EL, FM, DA, AG, CCor, BDR, CD, SG, MM, NP, GP, RMPA, ER, DS and CCol contributed to review & editing. GP and LM contributed to conceptualization. LM contributed to project administration and supervision.

711

712 **Competing interests**

713

714 The authors declare that they have no conflict of interest.

715

716 **Acknowledgements**

717

718 The authors acknowledge the MIUR (Italian Ministry of University) PON Ricerca e Innovazione 2014-2020 – PER-ACTRIS-
719 IT – “Potenziamento della componente italiana dell'Infrastruttura di Ricerca Aerosol, Clouds and Trace Gases Research;
720 CIR01_00015 - PER-ACTRIS-IT “Potenziamento della componente italiana della Infrastruttura di Ricerca Aerosol, Clouds
721 and Trace Gases Research Infrastructure - Rafforzamento del capitale umano” - Avviso MUR D.D. n. 2595 del 24.12.2019
722 Piano Stralcio “Ricerca e Innovazione 2015-2017” and CIR01_00019 - PRO-ICOS_MED “Potenziamento della Rete di
723 Osservazione ICOS-Italia nel Mediterraneo - Rafforzamento del capitale umano” - Avviso MUR D.D. n. 2595 del 24.12.2019
724 Piano Stralcio “Ricerca e Innovazione 2015-2017”.The authors also acknowledge the IR0000032 – ITINERIS, Italian
725 Integrated Environmental Research Infrastructures System (D.D. n. 130/2022 - CUP B53C22002150006) Funded by EU -
726 Next Generation EU PNRR- Mission 4 “Education and Research” - Component 2: “From research to business” - Investment
727 3.1: “Fund for the realisation of an integrated system of research and innovation infrastructures” and ATMO-
728 ACCESS (Access to Atmospheric Research Facilities) Funded in the frame of the programme H2020-EU.1.4.1.2 Grant
729 Agreement n. 101008004 – (1 April 2021 – 31 March 2025)..The authors also acknowledge the Joint Research Unit ACTRIS-
730 Italy funded by the Italian Ministry of University and Research and the people of the ACTRIS Topical Centre CAIS-ECAC
731 (Centre for Aerosol In-Situ Measurement – European Center for Aerosol Calibration and Characterization) for their detailed
732 advice and individual help setting up the aerosol in-situ measurement program according to the ACTRIS standard procedures.

733

734

References

- Allen, A. G., Nemitz, E., Shi J. P., Harrison R. M., and Greenwood, J. C.: Size distribution of trace metals in atmospheric aerosols in the United Kingdom, *Atmos. Environ.*, 35, 4581–4591, [http://dx.doi.org/10.1016/S1352-2310\(01\)00190-X](http://dx.doi.org/10.1016/S1352-2310(01)00190-X), 2001.
- Aydin, F., Aydin, I., Erdoğan, S., Akba, O., Isik, B., & Hamamci, C.: Chemical Characteristics of Settled Particles during a Dust-Storm. *Pol. J. Environ. Stud.*, 21, 533-537, 2012.
- Atabakhsh, S., Poulain, L., Chen, G., Canonaco, F., Prévôt, A. S. H., Pöhlker, M., Wiedensohler, A., and Herrmann, H.: A 1-year aerosol chemical speciation monitor (ACSM) source analysis of organic aerosol particle contributions from anthropogenic sources after long-range transport at the TROPOS research station Melpitz, *Atmos. Chem. Phys.*, , 23, 6963–6988, <https://doi.org/10.5194/acp-23-6963-2023>, 2023.
- Baars, H., Ansmann, A., Ohneiser, K., Haarig, M., Engelmann, R., Althausen, D., Hanssen, I., Gausa, M., Pietruczuk, A., Szkop, A., Stachlewska, I. S., Wang, D., Reichardt, J., Skupin, A., Mattis, I., Trickl, T., Vogelmann, H., Navas-Guzmán, F., Haefele, A., Acheson, K., Ruth, A. A., Tatarov, B., Müller, D., Hu, Q., Podvin, T., Goloub, P., Veselovskii, I., Pietras, C., Haeffelin, M., Fréville, P., Sicard, M., Comerón, A., Fernández García, A. J., Molero Menéndez, F., Córdoba-Jabonero, C., Guerrero-Rascado, J. L., Alados-Arboledas, L., Bortoli, D., Costa, M. J., Dionisi, D., Liberti, G. L., Wang, X., Sannino, A., Papagiannopoulos, N., Boselli, A., Mona, L., D'Amico, G., Romano, S., Perrone, M. R., Belegante, L., Nicolae, D., Grigorov, I., Gialitaki, A., Amiridis, V., Soupiona, O., Papayannis, A., Mamouri, R.-E., Nisantzi, A., Heese, B., Hofer, J., Schechner, Y. Y., Wandering, U., and Pappalardo, G.: The unprecedented 2017–2018 stratospheric smoke event: decay phase and aerosol properties observed with the EARLINET, *Atmos. Chem. Phys.*, 19, 15183–15198, <https://doi.org/10.5194/acp-19-15183-2019>, 2019.
- Baltensperger, U., Weingartner, E., Burtscher, H., and Keskinen, J.: Dynamic mass and surface area measurements, in: *Aerosol Measurement*, edited by: Baron, P.-A., and Willeke, K., John Wiley and Sons, New York, 387-418, 2001.
- Binietoglou, I., Basart, S., Alados-Arboledas, L., Amiridis, V., Argyrouli, A., Baars, H., Baldasano, J. M., Balis, D., Belegante, L., Bravo-Aranda, J. A., Burlizzi, P., Carrasco, V., Chaikovsky, A., Comerón, A., D'Amico, G., Filioglou, M., Granados-Muñoz, M. J., Guerrero-Rascado, J. L., Ilic, L., Kokkalis, P., Maurizi, A., Mona, L., Monti, F., Muñoz-Porcar, C., Nicolae, D., Papayannis, A., Pappalardo, G., Pejanovic, G., Pereira, S. N., Perrone, M. R., Pietruczuk, A., Posyniak, M., Rocadenbosch, F., Rodríguez-Gómez, A., Sicard, M., Siomos, N., Szkop, A., Terradellas, E., Tsekeri, A., Vukovic, A., Wandering, U., and Wagner, J.: A methodology for investigating dust model performance using synergistic EARLINET/AERONET dust concentration retrievals, *Atmos. Meas. Tech.*, 8, 3577–3600, <https://doi.org/10.5194/amt-8-3577-2015>, 2015.

764 Boselli, A., Caggiano, R., Cornacchia, C., Madonna, F., Macchiato, M., Mona, L., Pappalardo, G., and Trippetta, S.: Multi
 765 year sun-photometer measurements for aerosol characterization in a Central Mediterranean site, *Atmos. Res.*, 104, 98–110,
 766 <https://doi.org/10.1016/j.atmosres.2011.08.002>, 2012.

767 Bressi, M., Cavalli, F., Putaud, J. P., Fröhlich, R., Petit, J. E., Aas, W., Äijälä, M., Alastuey, A., Allan, J. D., Aurela, M., Beric,
 768 M., Bougiatioti, A., Bukowiecki, N., Canonaco, F., Crenn, V., Dusanter, S., Ehn, M., Elsasser, M. and Prevot, A. S. H.: A
 769 European aerosol phenomenology - 7: High-time resolution chemical characteristics of submicron particulate matter across
 770 Europe, *Atmos. Environ.*, 10, 100108 <https://doi.org/10.1016/j.aeaoa.2021.100108>, 2021.

771 Cavalli, F., Viana, M., Yttri, K. E., Genberg, J., and Putaud, J. P.: Toward a standardised thermal-optical protocol for measuring
 772 atmospheric organic and elemental carbon: the EUSAAR protocol, *Atmos. Meas. Tech.*, 3, 79–89, [https://doi.org/10.5194/amt-](https://doi.org/10.5194/amt-3-79-2010)
 773 [3-79-2010](https://doi.org/10.5194/amt-3-79-2010), 2010.

774 Cazorla, A., Bahadur, R., Suski, K. J., Cahill, J. F., Chand, D., Schmid, B., Ramanathan, V., and Prather, K. A.: Relating
 775 aerosol absorption due to soot, organic carbon, and dust to emission sources determined from in-situ chemical measurements,
 776 *Atmos. Chem. Phys.*, 13, 9337–9350, <https://doi.org/10.5194/acp-13-9337-2013>, 2013.

777 Chen, L. W. A., Watson, J. G., Chow, J. C., Green, M. C., Inouye, D., and Dick, K.: Wintertime particulate pollution episodes
 778 in an urban valley of the Western US: a case study, *Atmos. Chem. Phys.*, 12, 10051–10064, [https://doi.org/10.5194/acp-12-](https://doi.org/10.5194/acp-12-10051-2012)
 779 [10051-2012](https://doi.org/10.5194/acp-12-10051-2012), 2012.

780 Cubison, M. J., Ortega, A. M., Hayes, P. L., Farmer, D. K., Day, D., Lechner, M. J., Brune, W. H., Apel, E., Diskin, G. S.,
 781 Fisher, J. A., Fuelberg, H. E., Hecobian, A., Knapp, D. J., Mikoviny, T., Riemer, D., Sachse, G. W., Sessions, W., Weber, R.
 782 J., Weinheimer, A. J., Wisthaler, A., and Jimenez, J. L.: Effects of aging on organic aerosol from open biomass burning smoke
 783 in aircraft and laboratory studies, *Atmos. Chem. Phys.*, 11, 12049–12064, <https://doi.org/10.5194/acp-11-12049-2011>, 2011.

784 Deliverable 5.1: ACTRIS NF Labelling Plan,
 785 [https://www.actris.eu/sites/default/files/Documents/ACTRIS%20IMP/Deliverables/ACTRIS%20IMP_WP5_D5.1_ACTRIS](https://www.actris.eu/sites/default/files/Documents/ACTRIS%20IMP/Deliverables/ACTRIS%20IMP_WP5_D5.1_ACTRIS%20NF%20Labelling%20Plan.pdf)
 786 [%20NF%20Labelling%20Plan.pdf](https://www.actris.eu/sites/default/files/Documents/ACTRIS%20IMP/Deliverables/ACTRIS%20IMP_WP5_D5.1_ACTRIS%20NF%20Labelling%20Plan.pdf), last access: 24 November 2024

787 De Rosa, B., Amato, F., Amodeo, A., D’Amico, G., Dema, C., Falconieri, A., Giunta, A., Gumà-Claramunt, P., Kampouri, A.,
 788 Solomos, S., Mytilinaios, M., Papagiannopoulos, N., Summa, D., Veselovskii, I.; Mona, L.: Characterization of Extremely
 789 Fresh Biomass Burning Aerosol by Means of Lidar Observations, *Remote Sens.*, 14, 4984, <https://doi.org/10.3390/rs14194984>,
 790 2022.

791 Drinovec, L., Močnik, G., Zotter, P., Prévôt, A.-S.-H., Ruckstuhl, C., Coz, E., Rupakheti, M., Sciare, J., Müller, T.,
 792 Wiedensohler, A., and Hansen, A. D.: The “dual-spot” Aethalometer: an improved measurement of aerosol black carbon with
 793 real-time loading compensation, *Atmos. Meas. Tech.*, 8, 1965–1979, <https://doi.org/10.5194/amt-8-1965-2015>, 2015.

794 Dušan, J., Ďurčanská, D., Bujdos. M.: The contribution of road traffic to particulate matter and metals in air pollution in the
795 vicinity of an urban road, *Transport and Environment*, 50, 397-408, [https://doi: 10.1016/j.trd.2016.11.024](https://doi.org/10.1016/j.trd.2016.11.024), 2017

796 Esteve, A. R., Estellés, V., Utrillas, M. P., Martínez-Lozano, J. A.: In-situ integrating nephelometer measurements of the
797 scattering properties of atmospheric aerosols at an urban coastal site in western Mediterranean, *Atmos. Environ.*, 47, 43–50,
798 <https://doi.org/10.1016/j.atmosenv.2011.11.043>, 2012.

799 Fernandez, A. J., Sicard, M., Costa, M. J., Guerrero-Rascado, J. L., Gómez-Amo, J. L., Molero, F., Barragán, R., Basart, S.,
800 Bortoli, D., Bedoya-Velásquez, A. E., Utrillas, M. P., Salvador, P., Granados-Muñoz, M. J., Potes, M., Ortiz-Amezcu, P.,
801 Martínez-Lozano, J. A., Artíñano, B., Muñoz-Porcar, C., Salgado, R., Román, R., Rocadenbosch, F., Salgueiro, V., Benavent-
802 Oltra, J. A., Rodríguez-Gómez, A., Alados-Arboledas, L., Comerón, A., and Pujadas, M.: Extreme, wintertime Saharan dust
803 intrusion in the Iberian Peninsula: lidar monitoring and evaluation of dust forecast models during the February 2017 event,
804 *Atmos. Res.*, 228, 223–241, [https://doi.org/ 10.1016/j.atmosres.2019.06.007](https://doi.org/10.1016/j.atmosres.2019.06.007), 2019.

805 Freudenthaler, V., Esselborn, M., Wiegner, M., Heese, B., Tesche, M., Ansmann, A., Müller, D., Althausen, D., Wirth, M.,
806 Fix, A., Ehret, G., Knippertz, P., Toledano, C., Gasteiger, J., Garhammer, M., and Seefeldner, M.: Depolarization ratio profiling
807 at several wavelengths in pure Saharan dust during SAMUM 2006, *Tellus B.*, 61, 165–179, [https://doi.org/10.1111/j.1600-](https://doi.org/10.1111/j.1600-0889.2008.00396.x)
808 [0889.2008.00396.x](https://doi.org/10.1111/j.1600-0889.2008.00396.x), 2009.

809 Fröhlich, R., Cubison, M. J., Slowik, J. G., Bukowiecki, N., Prévôt, A. S. H., Baltensperger, U., Schneider, J., Kimmel, J. R.,
810 Gonin, M., Rohner, U., Worsnop, D. R., and Jayne, J. T.: The ToF-ACSM: a portable aerosol chemical speciation monitor
811 with TOFMS detection, *Atmos. Meas. Tech.*, 6 (11), 3225–3241, <https://doi.org/10.5194/amt-6-3225-2013>, 2013.

812 Gonçalves, C., Alves, C., Evtyugina, M., Mirante, F., Pio, C., Caseiro, A., Schmidl, C., Bauer, H., Carvalho, F.:
813 Characterisation of PM10 emissions from wood-stove combustion of common woods grown in Portugal, *Atmos. Environ.*, 44,
814 4474-4480, <https://doi.org/10.1016/j.atmosenv.2010.07.026>, 2010. <http://rsdi.regione.basilicata.it>, last access: 28 November
815 2023.

816 <https://www.actris.eu>, last access: 13 December 2023.

817 <https://www.atmo-access.eu/second-call-for-access/>, last access: 2 December 2023.

818 <https://ciao.imaa.cnr.it>, last access: 4 December 2023.

819 <https://www.imaa.cnr.it/en/projects/38-attivita/progetti/713-per-actris-it>, last access: 6 December 2023.

820 <https://www.permapure.com>, last access: 10 December 2023.

821 <https://tsi.com/home/> last access: 15 November 2024

822 [Monotube Dryer 700 \(MD-700\) - Perma Pure](#), last access 16 November 2024

823 <http://www.quattro-esse.it/Home.html>, last access: 24 November 2024

824 https://doi.org/10.57837/cnr-imaa/ares/actris-earlinet/level3/climatological/2000_2019/pot last access: 25 November 2024

825 Huang, R. J., Yang, L., Cao, J., Chen, Y., Chen, Q., Li, Y., Duan, J., Zhu, C., Dai, W., Wang, K.: Brown carbon aerosol
826 in urban Xi'an, northwest China: The composition and light absorption properties. *Environ. Sci. Technol.*, 52(12), 6825–33.
827 <https://doi.org/10.1021/acs.est.8b02386>, 2018.

828 Ilić, L., Jovanović, A., Kuzmanoski, M., Lazić, L., Madonna, F., Rosoldi, M., Mytilinaios, M., Marinou, E., and Ničković, S.:
829 Mineralogy sensitive immersion freezing parameterization in DREAM, *J. Geophys. Res. Atmos.*, 127, e2021JD035093,
830 <https://doi.org/10.1029/2021JD035093>, 2022.

831 IPCC (2021). Aerosols and their impact on climate and human health. In *Climate Change 2021: The Physical Science Basis*.
832 Contribution of Working Group I to the Sixth Assessment Report of the Intergovernmental Panel on Climate Change (IPCC).
833 Cambridge University Press.

834 Kim, H. K., Choi, Y., and Ghim, Y. S.: Characterization of volatilization of filter-sampled PM_{2.5} semi-volatile inorganic ions
835 using a backup filter and denuders, *Aerosol Air Qual. Res.*, 15, 814–820, <https://doi.org/10.4209/aaqr.2014.09.0213>, 2015.

836 Laj, P., Myhre, C. L., Riffault, V., Amiridis, V., Fuchs, H., Eleftheriadis, K., Petäjä, T., Salameh, T., Kivekäs, N., Juurola, E. E.,
837 Saponaro, G., Philippin, S., Cornacchia, C., Arboledas, L. A., Baars, H., Claude, A., De Mazière, M., Dils, B., Dufresne, M.,
838 Enameliou, N., Favez, O., Fiebig, M., Haeffelin, M., Hermann, H., Höhler, K., Illmann, N., Kreuter, A., Ludewig, E., Marinou, E.,
839 Möhler, O., Mona, L., Murberg, L. E., Vicolae, D., Novelli, A., O'Connor, E., Ohneiser, K., Petracca Altieri, R. M., Picquet-Varrault,
840 B., Van Pinxteren, D., Pospichal, B., Putaud, J.-P., Reimann, S., Siomos, N., Stachlewska, I., Tillmann, R., Voudori, K. A.,
841 Wandinger, U., Wiedensohler, A., Apituley, A., Comerón, A., Gysel-Beer, M., Mihalopoulos, N., Nikolova, N., Pietruczuk, A.,
842 Sauvage, S., Sciare, J., Skov, H., Svendby, T., Swietlicki, E., Tonev, D., Vaughan, G., Zdimal, V., Baltensperger, U., Doussin, J.-F.,
843 Kulmala, M., Pappalardo, G., Sundet, S. S., Vana, M.: Aerosol, Clouds and Trace Gases Infrastructure (ACTRIS); The European
844 Research Infrastructure Supporting Atmospheric Science, *BAMS*, E1098-E1136, <https://doi.org/10.1175/BAMS-D-23-0064.1>,
845 2024.

846 Levin, Z., Ganor, E., and Gladstein, V.: The effects of desert particles coated with sulphate on rain formation in the Eastern
847 Mediterranean, *J. Appl. Meteorol.*, 35, 1511–1523, [https://doi.org/10.1175/15200450\(1996\)035<1511:TEODPC>2.0.CO;2](https://doi.org/10.1175/15200450(1996)035<1511:TEODPC>2.0.CO;2),
848 1996.

849 Levin, Z., Teller, A., Ganor, E. and Yin, Y.: On the interactions of mineral dust, sea-salt particles, and clouds: a measurement
850 and modeling study from the Mediterranean Israeli Dust Experiment campaign, *J. Geophys. Res.*, 110, D20202,
851 <https://doi.org/10.1029/2005JD005810>, 2005.

852 Lopatin, A., Dubovik, O., Chaikovsky, A., Goloub, P., Lapyonok, T., Tanré, D., and Litvinov, P.: Enhancement of aerosol
853 characterization using synergy of lidar and sun-photometer coincident observations: the GARRLiC algorithm, *Atmos. Meas.*
854 *Tech.*, 6, 2065–2088, <https://doi.org/10.5194/amt-6-2065-2013>, 2013.

855 Madonna, F., Amodeo, A., Cornacchia, C., D'Amico, G., Mona, L., Pandolfi, M., Pappalardo, G., and Cuomo, V.:
856 Multichannel microwave radiometer and water vapour Raman lidar: comparisons and synergies, *AITinforma - Rivista Italiana*
857 *di telerilevamento*, 35, 115–130, 2006.

858 Madonna F., Amodeo, A., D'Amico, G., Mona, L., and Pappalardo, G.: Observation of non-spherical ultragiant aerosol using
859 a microwave radar, *Geophys. Res. Lett.*, 37, L21814, doi:10.1029/2010GL044999, 2010.

860 Madonna, F., Amodeo, A., Boselli, A., Cornacchia, C., Cuomo, V., D'Amico, G., Giunta, A., Mona, L., and Pappalardo, G.:
861 CIAO: the CNR-IMAA advanced observatory for atmospheric research, *Atmos. Meas. Tech.*, 4, 1191–1208,
862 <https://doi.org/10.5194/amt-4-1191-2011>, 2011.

863 Madonna, F., Amato, F., Vande Hey, J., and Pappalardo, G.: Ceilometer aerosol profiling versus Raman lidar in the frame of
864 the INTERACT campaign of ACTRIS, *Atmos. Meas. Tech.*, 8, 2207–2223, <https://doi.org/10.5194/amt-8-2207-2015>, 2015.

865 Mahowald, N., Albani, S., Kok, J. F., Engelstaeder, S., Scanza, R., Ward, D. S. and Flanner, M. G.: The size distribution of
866 desert dust aerosols and its impact on the Earth system, *Aeolian Res.*, 15, 53–71, <https://doi.org/10.1016/j.aeolia.2013.09.002>,
867 2014.

868 Mărmureanu, L., Marin, C.A., Andrei, S., Antonescu, B., Ene, D., Boldeanu, M., Vasilescu, J., Vițelaru, C., Cadar, O., Levei,
869 E.: Orange Snow—A Saharan Dust Intrusion over Romania During Winter Conditions. *Remote Sens.*, 11, 2466.
870 <https://doi.org/10.3390/rs11212466>, 2019

871 Matthias, V., Balis, D., Bosenberg, J., Eixmann, R., Iarlori, M., Komguem, L., Mattis, I., Papayannis, A., Pappalardo, G.,
872 Perrone, M. R., and Wang, X.: Vertical aerosol distribution over Europe: Statistical analysis of Raman lidar data from 10
873 European Aerosol Research Lidar Network (EARLINET) stations, *J. Geophys. Res. Atmos.*, 109 (D18), D18201,
874 <https://doi.org/10.1029/2004JD004638>, 2004.

875 Middlebrook, A. M., Bahreini, R., Jimenez, J. L., and Canagaratna, M. R.: Evaluation of composition-dependent collection
876 efficiencies for the Aerodyne Aerosol Mass Spectrometer using field data, *Aerosol Sci. Tech.*, 46, 258–271,
877 <https://doi.org/10.1080/02786826.2011.620041>, 2012.

878 Molero, F., Pujadas, M., and Artinano, B.: Study of the Effect of Aerosol Vertical Profile on Microphysical Properties Using
879 GRASP Code with Sun/Sky Photometer and Multiwavelength Lidar Measurements, *Remote Sens.*, 12(24) 4072-4089,
880 <https://doi.org/10.3390/rs12244072>, 2020.

881 Mona, L., Amodeo, A., Pandolfi, M., and Pappalardo, G.: Saharan dust intrusions in the Mediterranean area: three years of
882 Raman lidar measurements, *J. Geophys. Res.*, 111, D16203, <https://doi.org/10.1029/2005JD006569>, 2006.

883 Mona, L., Pappalardo, G., Amodeo, A., D'Amico, G., Madonna, F., Boselli, A., Giunta, A., Russo, F., and Cuomo, V.: One
884 year of CNR-IMAA multi-wavelength Raman lidar measurements in coincidence with CALIPSO overpasses: Level 1 products
885 comparison, *Atmos. Chem. Phys.*, 9, 7213–7228, <https://doi.org/10.5194/acp-9-7213-2009>, 2009.

886 Mona, L., Amodeo, A., D'Amico, G., Giunta, A., Madonna, F., and Pappalardo, G.: Multi-wavelength Raman lidar
887 observations of the Eyjafjallajökull volcanic cloud over Potenza, southern Italy, *Atmos. Chem. Phys.*, 12, 2229–2244,
888 <https://doi.org/10.5194/acp-12-2229-2012>, 2012.

889 Mona, L., Papagiannopoulos, N., Basart, S., Baldasano, J., Biniatoglou, I., Cornacchia, C., and Pappalardo, G.: EARLINET
890 dust observations vs. BSC-DREAM8b modeled profiles: 12-year-long systematic comparison at Potenza, Italy, *Atmos. Chem.*
891 *Phys.*, 14, 8781–8793, <https://doi.org/10.5194/acp-14-8781-2014>, 2014.

892 Mona, L., Amiridis, V., Cuevas, E., Gkikas, A., Trippetta, S., Vendenbussche, S., Benedetti, a., Dagsson-Waldhauserova, P.,
893 Formenti, P., Haeferle, A., Kazadzis, S., Knippertz, P., Laurent, B., Madonna, F., Nickovic, S., Papagiannopoulos, N.,
894 Pappalardo, G., García-Pando, C. P., Popp, T., Rodríguez, S., Sealy, A., Sugimoto, N., Terradellas, E., Vimic, A. V., Weinzierl,
895 B., Basart, S.: Observing Mineral Dust in Northern Africa, the Middle East, and Europe: Current Capabilities and Challenges
896 ahead for the Development of Dust Services. *Bull. Amer. Meteor. Soc.*, 104, E2223–E2264, [https://doi.org/10.1175/BAMS-D-](https://doi.org/10.1175/BAMS-D-23-0005.1)
897 [23-0005.1](https://doi.org/10.1175/BAMS-D-23-0005.1), 2023.

898 Monteiro, A., Basart, S., Kazadzis, S., Votsis, A., Gkikas, A., Vandenbussche, S., Tobias, A., Gama, C., García-Pando, C. P.,
899 Terradellas, E., Notas, G., Middleton, N., Kushta, J., Amiridis, V., Lagouvardos, K., Kosmopoulos, P., Kotroni, V., Kanakidou,
900 M., Mihalopoulos, N., Kalivitis, N., Dagsson-Waldhauserová, P., El-Askary, H., Sievers, K., Giannaros, T., Mona, L., Hirtl,
901 M., Skomorowski, P., Virtanen, T.H., Christoudias, T., Di Mauro, B., Trippetta, S., Kutuzov, S., Meinander, O., Nickovic, S.:
902 Multi-sectoral impact assessment of an extreme African dust episode in the Eastern Mediterranean in March 2018, *Sci Total*
903 *Environ.*, 843, 156861. doi: 10.1016/j.scitotenv.2022.156861, 2022.

904 Nelson, J., Chalbot, M-CG., Tsiodra, I., Mihalopoulos, N., Kavouras, IG.: Physicochemical characterization of personal
905 exposures to smoke aerosol and PAHs of wildland firefighters in prescribed fires. *Expo. Health.*, 13, 105–18
906 <https://doi.org/10.1007/s12403-020-00366-5>, 2021.

907 Ng, N. L., Herndon, S. C., Trimborn, A., Canagaratna, M. R., Croteau, P. L., Onasch, T. B., Sueper, D., Worsnop, D. R.,
908 Zhang, Q., Sun, Y. L., and Jayne, J. T.: An aerosol chemical speciation monitor (ACSM) for routine monitoring of the
909 composition and mass concentrations of ambient aerosol, *Aerosol Sci. Tech.*, 45 (7), 780–794,
910 <https://doi.org/10.1080/02786826.2011.560211>, 2011.

911 Nicolae, D., Vasilescu, J., Talianu, C., Biniatoglou, I., Nicolae, V., Andrei, S., and Antonescu, B.: A neural network aerosol-
912 typing algorithm based on lidar data, *Atmos. Chem. Phys.*, 18, 14511–14537, <https://doi.org/10.5194/acp-18-14511-2018>,
913 2018.

914 Ohneiser, K., Ansmann, A., Chudnovsky, A., Engelmann, R., Ritter, C., Veselovskii, I., Baars, H., Gebauer, H., Griesche, H.,
915 Radenz, M., Hofer, J., Althausen, D., Dahlke, S., and Maturilli, M.: The unexpected smoke layer in the High Arctic winter

916 stratosphere during MOSAiC 2019–2020, *Atmos. Chem. Phys.*, 21, 15783–15808, [https://doi.org/10.5194/acp-21-15783-](https://doi.org/10.5194/acp-21-15783-2021)
917 2021, 2021.

918 Olson, M. R., Victoria Garcia, M., Robinson, M. A., Van Rooy, P., Dietenberger, M. A., Bergin, M., Schaefer, J. J.: Investigation of black and brown carbon multiple wavelength-dependent light absorption from biomass and fossil fuel
919 combustion source emissions. *J. Geophys. Res. Atmos.*, 120, 6682–97 <https://doi.org/10.1002/2014JD022970>, 2015.

921 Pacifico, L. R., Pizzolante, A., Guarino, A., Iannone, A., Esposito, M., Albanese, S.: Wildfire as a Source of Potentially Toxic
922 Elements (PTSe) in Soil: A Case Study from Campania Region (Italy), *Int. J. Environ. Res. Public Health*, 20, 4513,
923 <https://doi.org/10.3390/ijerph20054513>, 2023.

924 Pakkanen, T. A., Loukkola, K., Korhonen, C. H., Aurela, M., Makela, T., Hillamo, R. E., Aarnio, P., Koskentalo, T., Kousa,
925 A. and Maenhaut, W.: Sources and chemical composition of atmospheric fine and coarse particles in the Helsinki area, *Atmos.*
926 *Environ.*, 35, 5381–5391, <http://hdl.handle.net/1854/LU-138499>, 2001.

927 Papagiannopoulos, N., Mona, L., Amodeo, A., D’Amico, G., Gumà Claramunt, P., Pappalardo, G., Alados-Arboledas, L.,
928 Guerrero-Rascado, J. L., Amiridis, V., Kokkalis, P., Apituley, A., Baars, H., Schwarz, A., Wandinger, U., Biniotoglou, I.,
929 Nicolae, D., Bortoli, D., Comerón, A., Rodríguez-Gómez, A., Sicard, M., Papayannis, A., and Wiegner, M.: An automatic
930 observation-based aerosol typing method for EARLINET, *Atmos. Chem. Phys.*, 18, 15879–15901,
931 <https://doi.org/10.5194/acp-18-15879-2018>, 2018.

932 Pappalardo, G., Amodeo, A., Mona, L., Pandolfi, M., Pergola, N., and Cuomo, V.: Raman lidar observations of aerosol emitted
933 during the 2002 Etna eruption, *Geophys. Res. Lett.*, 31, L05120, <https://doi.org/10.1029/2003GL019073>, 2004a.

934 Pappalardo, G., Amodeo, A., Pandolfi, M., Wandinger, U., Ansmann, A., Bosenberg, J., Matthias, V., Amiridis, V., de Tomasi,
935 F., Frioud, M., Iarlori, M., Komguem, L., Papayannis, A., Rocadenbosch, F., and Wang, X.: Aerosol lidar intercomparison in
936 the framework of EARLINET, Part III. Raman lidar algorithm for aerosol extinction, backscatter and lidar ratio, *Appl. Opt.*,
937 43(28), 5370–5385, <https://doi.org/10.1364/AO.43.000977>, 2004b.

938 Pappalardo, G., Mona, L., D’Amico, G., Wandinger, U., Adam, M., Amodeo, A., Ansmann, A., Apituley, A., Alados
939 Arboledas, L., Balis, D., Boselli, A., Bravo-Aranda, J. A., Chaikovsky, A., Comeron, A., Cuesta, J., De Tomasi, F.,
940 Freudenthaler, V., Gausa, M., Giannakaki, E., Giehl, H., Giunta, A., Grigorov, I., Groß, S., Haeffelin, M., Hiebsch, A., Iarlori,
941 M., Lange, D., Linné, H., Madonna, F., Mattis, I., Mamouri, R-E., McAuliffe, M. A. P., Mitev, V., Molero, F., Navas-Guzman,
942 F., Nicolae, D., Papayannis, A., Perrone, M. R., Pietras, C., Pietruczuk, A., Pisani, G., Preißler, J., Pujadas, M., Rizi, V., Ruth,
943 A. A., Schmidt, J., Schnell, F., Seifert, P., Serikov, I., Sicard, M., Simeonov, V., Spinelli, N., Stebel, K., Tesche, M., Trickl,
944 T., Wang, X., Wagner, F., Wiegner, M., Wilson, K. M.: Four-dimensional distribution of the 2010 Eyjafjallajökull volcanic
945 cloud over Europe observed by EARLINET, *Atmos. Chem. Phys.*, 13, 4429–4450, [doi:10.5194/acp-13-4429-2013](https://doi.org/10.5194/acp-13-4429-2013), 2013.

946 Peters, T. M., and Leith, D.: Concentration measurement and counting efficiency of the aerodynamic particle sizer 3321, J.
 947 Aerosol Sci., 34(5), 627–634, [https://doi.org/10.1016/S0021-8502\(03\)00030-2](https://doi.org/10.1016/S0021-8502(03)00030-2), 2003.

948 Petzold, A., Ogren, J. A., Fiebig, M., Laj, P., Li, S. M., Baltensperger, U., Holzer-Popp, T., Kinne, S., Pappalardo, G.,
 949 Sugimoto, N., Wehrli, C., Wiedensohler, A., and Zhang, X. Y.: Recommendations for reporting “black carbon” measurements,
 950 Atmos. Chem. Phys., 13, 8365–8379, <https://doi.org/10.5194/acp-13-8365-2013>, 2013.

951 Pio, C., Cerqueira, M., Harrison, R. M., Nunes, T., Mirante, F., Alves, C., Oliveira, C., Sanchez de la Campa, A., Artíñano,
 952 B., and Matos, M.: OC/EC ratio observations in Europe: Re-thinking the approach for apportionment between primary and
 953 secondary organic carbon, Atmos. Environ., 45, 6121–6132, <https://doi.org/10.1016/j.atmosenv.2011.08.045>, 2011.

954 Pöschl, U.: Atmospheric Aerosols: Composition, Transformation, Climate and Health Effects. Angew. Chem. Int. Ed., 44:
 955 7520–7540. <https://doi.org/10.1002/anie.200501122>, 2005.

956 Rajšić, S., Mijić, Z., Tasić, M., Radenković, M., and Joksić, J.: Evaluation of the levels and sources of trace elements in urban
 957 particulate matter, Environ. Chem. Lett., 6, 95–100, <https://doi.org/10.1007/s10311-007-0115-0>, 2008.

958 Ren-Jian, Z., Kin-Fai, H., & Zhen-Xing, S. (2012). The Role of Aerosol in Climate Change, the Environment, and Human
 959 Health. *Atmospheric and Oceanic Science Letters*, 5(2), 156–161. <https://doi.org/10.1080/16742834.2012.11446983>.

960 Ridolfi, M., Blum, U., Carli, B., Catoire, V., Ceccherini, S., Claude, H., De Clercq, C., Fricke, K. H., Friedl-Vallon, F., Iarlori,
 961 M., Keckhut, P., Kerridge, B., Lambert, J.-C., Meijer, Y. J., Mona, L., Oelhaf, H., Pappalardo, G., Pirre, M., Rizi, V., Robert,
 962 C., Swart, D., von Clarmann, T., Waterfall, A., and Wetzol, G.: Geophysical validation of temperature retrieved by the ESA
 963 processor from MIPAS/ENVISAT atmospheric limb-emission measurements, Atmos. Chem. Phys., 7, 4459–4487,
 964 <https://doi.org/10.5194/acp-7-4459-2007>, 2007.

965 Rodriguez-Navarro, C., di Lorenzo, F., and Elert, K.: Mineralogy and physicochemical features of Saharan dust wet deposited
 966 in the Iberian Peninsula during an extreme red rain event, Atmos. Chem. Phys., 18, 10089–10122, <https://doi.org/10.5194/acp-18-10089-2018>, 2018.

968 Rosoldi, M., Coppa, G., Merlone, A., Musacchio, C., and Madonna, F.: Intercomparison of Vaisala RS92 and RS41
 969 Radiosonde Temperature Sensors under Controlled Laboratory Conditions, Atmosphere, 13, 773,
 970 <https://doi.org/10.3390/atmos13050773>, 2022.

971 Sandradewi, J., Prévôt, A. S. H., Szidat, S., Perron, N., Alfarra, M., Lanz, V. A., Weingartner, E., and Baltensperger, U.: Using
 972 Aerosol Light Absorption Measurements for the Quantitative Determination of Wood Burning and Traffic Emission
 973 Contributions to Particulate Matter, Environ. Sci. Technol., 42, 3316–3323, <https://doi.org/10.1021/es702253m>, 2008.

974 Sawamura, P., Vernier, J. P., Barnes, J. E., Berkoff, T. A., Welton, E. J., Alados-Arboledas, L., Navas-Guzmán, F., Pappalardo,
 975 G., Madonna, F.: Stratospheric AOD after the 2011 eruption of Nabro volcano measured by lidar over the Northern
 976 Hemisphere, Environ. Res. Lett., 7, 031001, <https://doi.org/10.1088/1748-9326/7/3/034013>, 2012.

977 Schmid, O., Karg, E., Hagen, D. E., Whitefield, P. D., and Ferron, G. A.: On the effective density of non-spherical particles as
 978 derived from combined measurements of aerodynamic and mobility equivalent size, *J. Aerosol Sci.*, 38(4), 431–443,
 979 <https://doi.org/10.1016/j.jaerosci.2007.01.002>, 2007.

980 Schmidl, C., Marr, I. L., Caseiro, A., Kotianová, P., Berner, A., Bauer, H., Kasper-Giebl, A., Puxbaum, H.: Chemical
 981 characterization of fine particle emissions from wood stove combustion of common woods growing in mid-European Alpine
 982 regions, *Atmos. Environ.*, 42, 126–141, <https://doi.org/10.1016/j.atmosenv.2007.09.028>, 2008.

983 Sirignano, C., Riccio, A., Chianese, E., Ni, H., Zenker, K., D’Onofrio, A., Meijer, H. A. J., and Dusek, U.: High Contribution
 984 of Biomass Combustion to PM_{2.5} in the City Centre of Naples (Italy), *Atmosphere*, 10, 451,
 985 <https://doi.org/10.3390/atmos10080451>, 2019.

986 Sokolik, I. N., and Toon, O. B.: Direct radiative forcing by anthropogenic airborne mineral aerosols, *Nature*, 381, 681–683,
 987 <https://doi.org/10.1038/381681a0>, 1996.

988 Soupiona, O., Papayannis, A., Kokkalis, P., Foskinis, R., Sánchez Hernández, G., Ortiz-Amezcu, P., Mylonaki, M.,
 989 Papanikolaou, C.-A., Papagiannopoulos, N., Samaras, S., Groß, S., Mamouri, R.-E., Alados-Arboledas, L., Amodeo, A., and
 990 Psiloglou, B.: EARLINET observations of Saharan dust intrusions over the northern Mediterranean region (2014–2017):
 991 properties and impact on radiative forcing, *Atmos. Chem. Phys.*, 20, 15147–15166, [https://doi.org/10.5194/acp-20-15147-](https://doi.org/10.5194/acp-20-15147-2020)
 992 2020, 2020.

993 Veselovskii, I., Dubovik, O., Kolgotin, A., Korenskiy, M., Whiteman, D. N., Allakhverdiev, K., and Huseyinoglu, F.: Linear
 994 estimation of particle bulk parameters from multi-wavelength lidar measurements, *Atmos. Meas. Tech.*, 5, 1135–1145,
 995 [doi:10.5194/amt-5-1135-2012](https://doi.org/10.5194/amt-5-1135-2012), 2012.

996 Viana, M., Chi, X., Maenhaut, W., Cafmeyer, J., Querol, X., Alastuey, A., Mikuška, P., and Večeřa, Z.: Influence of sampling
 997 artefacts on measured PM, OC, and EC Levels in carbonaceous aerosols in an urban area, *Aerosol Sci. Tech.*, 40 (2), 107–117,
 998 <https://doi.org/10.1080/02786820500484388>, 2006.

999 Villani, M. G., Mona, L., Maurizi, A., Pappalardo, G., Tiesi, A., Pandolfi, M., D’Isidoro, M., Cuomo, V., Tampieri, F.:
 1000 Transport of volcanic aerosol in the troposphere: the case study of the 2002 Etna plume, *J. Geophys. Res.*, Vol. 111, No. D21,
 1001 D21102, [doi:10.1029/2006JD007126](https://doi.org/10.1029/2006JD007126), 2006.

1002 Vratolis, S., Fetfatzis, P., Argyrouli, A., Soupiona, O., Mylonaki, M., Maroufidis, J., Kalogridis, A. C., Manousakas, M.,
 1003 Bezantakos, S., Binietoglou, I., Labzovskii, L. D., Solomos, S., Papayannis, A., Močnik, G., O’Connor, E., Müllerf, D.,
 1004 Tzani, C. G., and Eleftheriadis, K.: Comparison and complementary use of in situ and remote sensing aerosol measurements
 1005 in the Athens Metropolitan Area, *Atmos. Environ.*, 228 (117439), <https://doi.org/10.1016/j.atmosenv.2020.117439>, 2020.

1006 Wiedensohler, A., Birmili, W., Putaud, J. P., and Ogren, J.: Recommendations for Aerosol Sampling, in: *Aerosol Science:*
 1007 *Technology and Applications*, First Edition, edited by: Colbeck, I., and Lazaridis, M., John Wiley & Sons, Ltd., 45–59,

1008 <https://doi.org/10.1002/9781118682555.ch3>, 2014.WMO/GAW Aerosol Measurement Procedures, Guidelines and
1009 Recommendations 2nd Edition, No. 227, 2016.

1010 Zhi, M., Zhang, X., Zhang, K., Ussher, S. J., Lv, W., Li, J., Gao, J., Luo, Y., Meng, F.,: The characteristics of atmospheric
1011 particles and metal elements during winter in Beijing: Size distribution, source analysis, and environmental risk assessment,
1012 Ecotoxicol. Environ. Saf., 211, 111937, <https://doi.org/10.1016/j.ecoenv.2021.111937>, 2021.

1013 Zhou, C. W., Huang, H., and Cao, J. J.: Summary of basic characteristics of atmospheric aerosol carbonaceous, Environ. Pollut.
1014 Control, 28, 270-274, 2006.

1015 Zhao, Q., Huob, J., Yanga, X., Fub, Q., Duanb, Y., Liua, Y., Linb, Y., Zhang, Q.: Chemical characterization and source
1016 identification of submicron aerosols from a year-long real-time observation at a rural site of Shanghai using an Aerosol
1017 Chemical Speciation Monitor, Atmos. Res., 246, 105154, <https://doi.org/10.1016/j.atmosres.2020.105154>, 2020.

1018

1019